



**HAL**  
open science

## Electrochemical impedance spectroscopy

Shangshang Wang, Jianbo Zhang, Oumaïma Gharbi, Vincent Vivier, Ming Gao, Mark E Orazem

► **To cite this version:**

Shangshang Wang, Jianbo Zhang, Oumaïma Gharbi, Vincent Vivier, Ming Gao, et al.. Electrochemical impedance spectroscopy. *Nature Reviews Methods Primers*, 2021, 1, 41 (21p.). 10.1038/s43586-021-00039-w . hal-03258251

**HAL Id: hal-03258251**

**<https://hal.science/hal-03258251>**

Submitted on 11 Jun 2021

**HAL** is a multi-disciplinary open access archive for the deposit and dissemination of scientific research documents, whether they are published or not. The documents may come from teaching and research institutions in France or abroad, or from public or private research centers.

L'archive ouverte pluridisciplinaire **HAL**, est destinée au dépôt et à la diffusion de documents scientifiques de niveau recherche, publiés ou non, émanant des établissements d'enseignement et de recherche français ou étrangers, des laboratoires publics ou privés.

# ELECTROCHEMICAL IMPEDANCE SPECTROSCOPY

Shangshang Wang,<sup>1</sup> Jianbo Zhang,<sup>1</sup> Oumaïma Gharbi,<sup>2</sup> Vincent Vivier,<sup>2</sup> Ming Gao,<sup>3</sup> and Mark E. Orazem<sup>3†</sup>

<sup>1</sup>School of Vehicle and Mobility, Tsinghua University, Beijing, China

<sup>2</sup>Sorbonne Université, CNRS, Laboratoire Interfaces et Systèmes Electrochimiques (LISE), 4 place Jussieu, F-75005, Paris, France

<sup>3</sup>Department of Chemical Engineering, University of Florida, Gainesville, Florida, 32611 USA,

†Corresponding email: [morazem@che.ufl.edu](mailto:morazem@che.ufl.edu)

27 ABSTRACT

28 Electrochemical impedance spectroscopy (EIS) is a powerful tool to investigate properties of materials and  
29 electrode reactions. This Primer provides a guide to the use of EIS with a comparison to other  
30 electrochemical techniques. The analysis of impedance data for reduction of ferricyanide in a KCl  
31 supporting electrolyte is used to demonstrate the error structure for impedance measurements, the use  
32 of measurement and process models, as well as the sensitivity of impedance to the evolution of electrode  
33 properties. This Primer provides guidelines for experimental design, discusses the relevance of accuracy  
34 contour plots to wiring and instrumentation selection, and emphasizes the importance of the Kramers-  
35 Kronig relations to data validation and analysis. Applications of EIS to battery performance, metal and  
36 alloy corrosion, and electrochemical biosensors are highlighted. Electrochemical impedance  
37 measurements depend on both the mechanism under investigation and extrinsic parameters, such as the  
38 electrode geometry. Experimental complications are discussed, including the influence of nonstationary  
39 behaviour at low frequencies and the need for reference electrodes. Finally, emerging trends in  
40 experimental and interpretation approaches are also described.

41

## [H1] Introduction

Electrochemistry is a discipline encompassing all heterogeneous chemical reactions involving electron transfer, homogeneous reactions that influence reactions at electrode surfaces, properties of the interfaces (the double layer) and bulk properties of electrolytes. Electrochemical reactions are at the root of several research areas including energy conversion and storage, corrosion, sensors and biosensing applications, as well as the production of commodity materials such as aluminum and chlorine. The development of several electrochemical techniques such as cyclic voltammetry (CV), chronoamperometry and chronopotentiometry, scanning electrochemical microscopy (SECM), and electrochemical impedance spectroscopy (EIS), was required to enable studying these reactions across this broad range of application settings. Each of these techniques has expanded in recent decades, as a result of advances in instrumentation and modeling.<sup>1,2</sup>

From a mechanistic point of view, an electrochemical reaction at an electrode/electrolyte interface can be decomposed into a series of multi-step processes (mass transport, charge-transfer processes, adsorption), each occurring at distinct rates. The individual steps are time dependent and may occur at different time scales. Therefore, the use of transient techniques such as EIS, which enables the analysis of time-dependent mechanisms based on the response (current or potential) of the electrochemical system collected at selected frequencies, is required to facilitate evaluation of electrochemical systems. The EIS technique is broadly applicable because it can provide an understanding of the electrochemical mechanisms occurring at an electrified interface in a single measurement. These underlying mechanisms include those involved in operating commercial batteries, the corrosion of metals and alloys and electrochemical biosensors.

Textbooks, monographs<sup>2-5</sup> and review articles have been dedicated to EIS that are specific to the applications.<sup>6-12</sup> The history of EIS has also been retraced,<sup>13,14</sup> highlighting the evolution of the technique from the first measurement of electrolyte conductivity using alternating current in the mid-19<sup>th</sup> century<sup>15,16</sup> to the measurement of **interfacial capacitance [G]**<sup>17</sup> or the measurement of diffusivity.<sup>18</sup> EIS has benefited from the development of instruments, such as the first **potentiostats [G]** and the **rotating disk electrode [G]**. Potentiostats enable the control of the working-electrode potential referenced to an electrode at its equilibrium redox potential<sup>19</sup> and the rotating disk electrode affords the well-defined transport of reactants and products to the electrode surface.<sup>20</sup> The development of mathematical models, such as those for porous electrodes that describe the impedance response as a function of the pore geometry in the presence or absence of electrochemical reactions, have enabled a better understanding

73 of complex electrochemical systems.<sup>21,22</sup> EIS has also allowed for better comprehension of intermediate  
 74 adsorption on electrode surfaces,<sup>23,24</sup> particularly for multi-step mechanisms, including electrochemical  
 75 reactions coupled by adsorbed reaction intermediates, electrochemical reactions coupled with  
 76 homogeneous or heterogeneous chemical reactions, and photoelectrochemical reactions<sup>25,26</sup>. Examples  
 77 include iron dissolution in an acidic solution<sup>27,28</sup> and corrosion of magnesium.<sup>29,30</sup> EIS is a technique of  
 78 choice for the study of porous electrodes<sup>21,22,31</sup> because the output is directly affected by the porosity of  
 79 the electrode, which may allow the pore size to be evaluated.<sup>32-34</sup> Together, advances in instrumentation  
 80 and models provide the capability for detecting multi-step mechanisms and define modern EIS.<sup>2,35</sup>

81 CV is often preferred to EIS for the study of electrochemical steps coupled with chemical reactions,  
 82 whose kinetics can be measured by varying the potential scan rate.<sup>36-39</sup> In contrast to CV where the entire  
 83 potential domain is scanned at a given scan rate, EIS offers the unique advantage of being able to perform  
 84 measurements at different potentials. Interestingly, the potential dependence of the charge-transfer  
 85 coefficient was inferred from EIS measurements on aromatic compounds with fast reaction kinetics,  
 86 revealing a good agreement with the predicted values using the Marcus theory for outer-sphere electron  
 87 transfers.<sup>40</sup> The potential dependence of the charge-transfer coefficient was also observed by CV, but it  
 88 requires the use of convolution sweep voltammetry<sup>41</sup> or the comparison of CV data (the shape of the  
 89 voltammogram, the peak separation, the peak current) to digital simulations.<sup>42</sup> CV and EIS are therefore  
 90 complementary techniques, and the choice of which technique is best to use depends on the process that  
 91 each user is seeking to characterize.

92 EIS is a type of transfer-function measurement, commonly used in the analysis of linear time-  
 93 invariant systems.<sup>2</sup> In the case of an electrochemical system, the main difficulty is that the system must  
 94 remain in a stationary state throughout the measurement. EIS uses a small-amplitude potential or current  
 95 periodic perturbation to excite the electrochemical system at different frequencies, as illustrated in Figure  
 96 1. By measuring the response (current or potential) of the system to this perturbation, a transfer function  
 97 is calculated that is the electrochemical impedance of the system in the case of an electrochemical cell.  
 98 The impedance  $Z$  can be expressed as<sup>2</sup>

$$Z(\omega) = \frac{\tilde{V}(\omega)}{\tilde{i}(\omega)} = \left| \frac{\tilde{V}(\omega)}{\tilde{i}(\omega)} \right| (\cos \phi(\omega) + j \sin \phi(\omega)) = Z_r + jZ_j \quad (1)$$

99 where  $\omega$  is the angular frequency, related to the frequency  $f$  in Hz by  $\omega = 2\pi f$ ,  $\phi$  is the phase angle  
 100 between the input and the output signals, and  $j = \sqrt{-1}$  is the imaginary number. The variables  $\tilde{V}$  and  $\tilde{i}$

101 are phasors, which are complex time-invariant numbers that account for the amplitude and phase of a  
102 sinusoidal function. The electrochemical impedance, as defined by equation (1), is a frequency-dependent  
103 complex number [G], whose real part  $Z_r$  is the resistance [G] and the imaginary part  $Z_j$  is the reactance  
104 [G]. Although the IUPAC conventions<sup>43</sup> holds that the real part should be represented by  $Z'$  and the  
105 imaginary part denoted by  $Z''$ , the use of primes is too easily confused with the notation for spatial  
106 derivatives in the engineering literature. Thus, the notation used in the present work is that the real part  
107 is denoted by a subscript “r” and the imaginary part is denoted by a subscript “j”.

108 EIS measurements should be designed to conform to the Kramers-Kronig relations (see **Box 1**), which  
109 are derived under the assumptions that the system under investigation is linear, stable, and causal (see  
110 **Box 2**). The perturbation amplitude required to achieve a linear response with an appropriate signal-to-  
111 noise ratio is generally determined experimentally for each system under study. Although a typical  
112 amplitude for potentiostatic modulation may be on the order of 10 mV, amplitudes as large as 1 V may  
113 be used for the impedance response of high-resistivity lubricating fluids. The Kramers-Kronig relations  
114 may be applied as a tool to determine which part of the measured frequency range is uncorrupted by  
115 instrument or nonstationary artifacts.

116 This Primer provides a description of the EIS technique and its principle, including the main aspects  
117 of the measurement procedure, data representation and analysis, but is not intended to cover the  
118 fundamentals of electrochemistry that can be found elsewhere<sup>1,44,45</sup>. The tools that will help design and  
119 perform a valid EIS measurement are described here with specific attention drawn to the choice of cell  
120 configuration, measurement settings (Experimentation) and data validation (Results). Several examples  
121 and applications are presented in order to introduce the different methods of data representation and  
122 interpretation. Finally, the challenges of this technique and an outlook of how EIS will likely evolve in the  
123 near future are presented and discussed.

## 124 [H1] EXPERIMENTATION

125 The use of EIS requires a number of steps, from the measurement procedure to data analysis. Despite  
126 the technique being incorporated into most modern potentiostat software, the first step is to make a  
127 correct measurement, which is the focus of this section. The EIS measurement system includes the  
128 samples and the cells, the instruments and the connection of cells with the instruments<sup>46</sup>.

## [H2] TEST SAMPLES AND CELLS

A cell with two, three or four electrodes can be used depending on the measurement to be carried out as shown in **Fig. 2**.<sup>1,47</sup> The two-electrode system (**Fig. 2a**) is used in cases where it is difficult to insert a reference electrode, such as batteries and fuel cells. The measured response is the sum of all contributions between the working electrode and the counter electrode, which complicates the interpretation of the impedance response. The three-electrode arrangement (**Fig. 2b**) is the classic device used for all analytical electrochemical measurements<sup>48,49</sup> that employs a working electrode, which is the sample of interest, a counter electrode and a reference electrode. The use of a reference electrode enables studying the working electrode response independent of the processes taking place at the counter-electrode. A four-electrode setup (**Fig. 2c**) is used for the characterization of electrolyte conductivity,<sup>50</sup> free-standing films,<sup>51</sup> embedded rebar in concrete<sup>52</sup> and the interface between two immiscible electrolyte solutions.<sup>53</sup> Two reference electrodes are positioned on either side of the interface to measure the potential and the two other electrodes allow for the passage of the current. The investigation of electrolytes or films without the confounding influence of working and counter-electrode impedances can be done using the four-electrode system. The chosen cell configuration depends on the system being evaluated.

The area of the counter electrode is normally much larger than that of the working electrode to minimize its contribution to the cell impedance. This size difference is especially important for two-electrode measurements in which the measured impedance includes contributions from both the working and counter electrodes. Although a uniform current and potential distribution on the working electrode are desirable, practical considerations often force the use of electrode configurations in which the current and potential distributions are not uniform. Frequency dispersion caused by non-uniform current and potential distributions distort the high-frequency impedance response, which complicates the interpretation of the impedance data. The geometry-induced frequency dispersion can be avoided by using small working electrodes or by eliminating the frequencies larger than the characteristic frequency

$$f_c = \frac{1}{2\pi R_e C} \quad (2)$$

where  $R_e$  is the high-frequency ohmic resistance [G] between the working and the reference electrodes and  $C$  is the capacitance [G] of the working electrode-electrolyte interface.<sup>54</sup>

The counter electrode is sometimes placed in a separate compartment to prevent its reaction products from interfering with the working electrode. This compartment is ionically connected with the working

158 electrode compartment, usually with a glass/ceramic frit or asbestos threads. The reference electrode  
159 should provide a stable potential measurement against which to control the potential of the working  
160 electrode. There are two approaches for the placement of the reference electrode. Placing the reference  
161 electrode close to the working electrode, such as using a Luggin tube in a glass cell<sup>55</sup> (**Fig. 2b**), results in a  
162 smaller contribution of the ohmic resistance. In contrast, placing the reference electrode far from the  
163 working electrode has the advantage that, for some geometries such as a disk electrode, a relationship  
164 exists between the electrolyte conductivity, the ohmic resistance and the electrode dimension,<sup>56</sup>

$$R_e = \frac{\pi r_0}{4 \kappa} \quad (3)$$

165 where  $r_0$  is the disk radius and  $\kappa$  is the electrolyte conductivity. The high-frequency ohmic resistance can  
166 be estimated using equation (3) because the electrolyte conductivity is often known, thus providing a  
167 check on the measurement quality.

168 High-frequency artifacts may appear when using an ordinary reference electrode for  
169 measurements taken using conventional three-electrode arrangements (**Fig. 2b**). The impedance of the  
170 reference electrode may decrease in the high-frequency region ( $> \sim 100$  kHz), increasing the current  
171 flowing through it, which would result in a fluctuation of the reference potential and afford abnormal  
172 impedance results. However, placing a capacitor (the value of which depends on the electrolyte  
173 conductivity) in series with a platinum wire that is connected in parallel to the reference electrode to  
174 bypass the high frequency component of current or noise can relieve this abnormality.<sup>57</sup>

## 175 [H2] INSTRUMENTATION

176 Along the course of developing the EIS measurement technique, instruments with different  
177 measurement principles have been proposed, including AC bridges,<sup>14,58</sup> Lissajous curves,<sup>2</sup> phase-sensitive  
178 detection and lock-in amplifier,<sup>59</sup> frequency-response analyzers,<sup>4,60</sup> Laplace transforms,<sup>61</sup> and wavelet  
179 transforms.<sup>62</sup> The dominant approach used by modern EIS instruments, provided by vendors such as  
180 Solartron, Biologic, Gamry, Metrohm and Zahner, falls in the category of frequency-response analyzers  
181 (FRA) that employ the orthogonality of sines and cosines to determine the real and imaginary parts of the  
182 complex impedance at a specified frequency. The discussion in the present work will accordingly  
183 emphasize FRAs.

## 184 [H3] ACCURACY CONTOUR PLOTS

185 The EIS accuracy depends on the measurement frequency and the impedance of the sample. Each  
186 device and associated cables can be characterized by an accuracy contour plot, which depicts the levels

187 of accuracy for the magnitude and phase angle of impedance based on the value of frequency and  
 188 magnitude of impedance. Such accuracy contour plots should be evaluated to see if the test sample of  
 189 interest falls into the area with adequate accuracy.<sup>63</sup> A generic accuracy contour plot for potentiostatic  
 190 modulation is shown in **Fig. 2d**. Line “A” is based on the minimum current resolution and can be moved  
 191 by changing the potential perturbation amplitude. The absolute high-impedance limits of a potentiostat  
 192 and associated cables can be obtained by measuring the impedance in which the wires are not connected,  
 193 simulating an infinite cell impedance. The result yields the effective capacitance of the leads and  
 194 instrumentation shown as line “B”. Line “C” corresponds to the maximum frequency capability of the  
 195 instrument. The absolute low-impedance limits can be obtained by measuring the impedance in which  
 196 the wires are shorted, simulating a zero cell-impedance. The result yields the effective inductance (line  
 197 “D”) and resistance (line “E”) of the leads and instrumentation. A zone is indicated in which impedance  
 198 measurements may be made with error less than 1% in magnitude and 2° in phase. A second zone  
 199 corresponds to errors larger than 10% and 10° for magnitude and phase, respectively. Measurements  
 200 outside the boundary formed by lines A through E are not possible.

201 The measured impedance can be represented by the electrical circuit (**Fig. 2e**), and the relationship  
 202 between measured impedance,  $Z_{\text{meas}}$ , and cell impedance,  $Z_{\text{cell}}$ , is given by

$$Z_{\text{meas}} = \frac{(R_{\text{wire}} + Z_{\text{L,wire}} + Z_{\text{cell}}) \times Z_{\text{C,wire}}}{R_{\text{wire}} + Z_{\text{L,wire}} + Z_{\text{cell}} + Z_{\text{C,wire}}} \quad (4)$$

203 where  $Z_{\text{C,wire}}$ ,  $Z_{\text{L,wire}}$  and  $R_{\text{wire}}$  are the impedances associated with the capacitance, inductance, and  
 204 the resistance of the wires, respectively. Instrument vendors usually use short shielded wires to reduce  
 205 the contribution of the wire capacitance and inductance and often provide accuracy contour plots with  
 206 wires coming with the instrument. However, the positions of the limits in accuracy contour plots are  
 207 strongly affected by the wires used to connect the instrument to the cell. To this end, users should always  
 208 generate a new accuracy and check it if they need to use longer wires for special purposes, such as  
 209 connecting the cell far away from the instrument.

210 The wires connecting the equipment and cells in EIS measurements form two loops, one includes  
 211 the two wires bearing the current and the other bears the two wires sensing the voltage (**Fig. 2f**). The  
 212 contribution of wire properties can be neglected and measured impedance is the same as the cell  
 213 impedance for most measurements. However, for systems exhibiting small impedance, the use of long  
 214 wires may give rise to high-frequency artifacts because the magnetic field generated by the alternating-  
 215 current-carrying leads will drive an alternating potential in the sense leads (**Fig. 2h**). This phenomenon is  
 216 called mutual inductance, which can be reduced by minimizing the loop area between the two current

217 wires and the two voltage wires via a tight-braided twist (**Fig. 2g**).<sup>64</sup> Another solution includes maximizing  
218 the distance between the current-carrying and the voltage-sensing wires.<sup>63</sup> Finally, orientating the clamp  
219 (bayonet) of the current and voltage wires in a cross configuration, that is perpendicular to each other,  
220 may help to further reduce this interaction.

### 221 [H3] SETTINGS

222 The quality of the impedance measurement is controlled by a series of parameters, including  
223 selection of potentiostatic or galvanostatic modulation, perturbation amplitude, frequency range and the  
224 number of cycles used to perform the measurement at each frequency. In principle, EIS can be obtained  
225 either by applying a current perturbation and measuring the potential response, in the galvanostatic mode,  
226 or by applying a potential perturbation and measuring the current response, in potentiostatic mode. The  
227 choice of potential or current regulation depends on the electrochemical systems, and a first criterion for  
228 this selection is the shape of the steady-state current potential curves, which should be generated before  
229 the EIS measurement as a best practice. When the slope of the current-potential curve is very sharp (for  
230 example, the dissolution of zinc), the galvanostatic mode is usually preferred because the potentiostatic  
231 mode may lead to overloading of the cell and the current measurement circuits of the potentiostat. For  
232 steep slopes of the current-potential curve, a small change in potential might lead to a large change in  
233 current. In general, galvanostatic impedance is more suitable for noninvasive probing of metal corrosion  
234 at the open-circuit potential and for measuring most high-energy electrochemical devices, where  
235 impedance is low and current levels are high. However, for electrochemical systems with larger  
236 impedance, the potentiostatic mode is generally employed.

237 The amplitude of the perturbing current or potential must be determined experimentally. The  
238 perturbation amplitude should be small enough to make the system linear, but as large as possible to get  
239 the best signal-to-noise ratio. Selection of the amplitude depends both on the polarization curve of the  
240 system and the noise level of the measurement system. The optimal perturbation amplitude is not  
241 necessarily the same over the entire frequency range and it may be compulsory to adapt it to make a good  
242 measurement because electrochemical systems involve different processes. For potentiostatic EIS mode,  
243 an AC potential signal with peak-to-peak amplitude of 5 to 15 mV is commonly used. However, for a  
244 system with large impedance or significant noise, the amplitude may be increased so long as linearity is  
245 assured. The potential changes associated with galvanostatic modulation depend on the frequency-  
246 dependent impedance of the system. As the impedance of the systems may change by orders of  
247 magnitude with frequency, the potential swing at low frequencies from a fixed galvanostatic modulation

248 may cause nonlinear behaviour. In this case, the amplitude of the current perturbation should be adjusted  
249 as a function of frequency. Algorithms for frequency-dependent galvanostatic modulation have been  
250 developed.<sup>65,66</sup> Distortions of the expected ellipse in low-frequency Lissajous plots (current as a function  
251 of potential) provide a good indicator for nonlinear response.<sup>67,68</sup> If distortions from a perfect ellipse are  
252 observed, the perturbation amplitude should be reduced. The monitoring of the spectral contents at  
253 higher harmonics of the response signal may also be used to determine the suitable range of perturbation  
254 amplitude. These experimental approaches are suitable for both potentiostatic and galvanostatic  
255 modulation.

256 The power of EIS lies in its ability to probe processes in systems across a wide frequency range.  
257 Ideally, the frequency range should be set to match the dynamic range of the system under study. Modern  
258 EIS instruments can easily cover a broader range from MHz to  $\mu$ Hz, spanning 12 orders of magnitudes. In  
259 practice, the accuracy of the equipment may drop significantly at high frequencies, as shown in **Fig. 2d**,  
260 and the measurement duration may become prohibitively long or the system may no longer be stationary  
261 in the low-frequency limit (see **Box 1**). As a result, the typical frequency range for electrochemical  
262 measurements, including energy conversion as well as storage device and corrosion, is 10 kHz to 10 mHz.  
263 Usually, 7 to 10 points per frequency decade (for example, from 100 Hz to 10 Hz), equally spaced  
264 logarithmically, are required for measuring an impedance spectrum with sufficient accuracy for a detailed  
265 data analysis. It is preferable to start the measurement from the high-frequency limit sweeping towards  
266 the low-frequency limit, because the operator has the opportunity to grasp the main behaviour of the  
267 system in a short period of time. If anything goes wrong, such as current overloads or excessively noisy  
268 signals, the operator can abort the measurement and make any necessary change or adjustment to the  
269 settings or the cell.

270 The stochastic error structure or noise level of the measurement is influenced by the number of  
271 cycles used to measure the impedance at each frequency. The precision of the measurement increases  
272 with the square-root of the integration cycles. This effect from the number of cycles used is particularly  
273 worthwhile at high frequencies because noise content is high and time overhead for repetition is low. At  
274 very low frequencies, this effect is less significant due to the increased time overhead on the one hand,  
275 and the change of the nature of the predominant noise from external electromagnetic interference to the  
276 system non-stationarity. For some instruments, an auto-integration mode is used to select the number of  
277 cycles, which is usually three or larger. In contrast, the user is allowed to choose between fast, normal

278 and low-noise options that influence the number of cycles used for the measurement for other  
279 instruments.

280 Introducing a delay of one or two cycles before the impedance measurement will help to reduce the  
281 errors because a transient response may occur in the cell during the change from one frequency to  
282 another. Similarly, there is usually a startup transient before the entire sequence of the measurement,  
283 which tends to corrupt the first frequency measured. A simple way of obviating this problem is to ignore  
284 the first frequency in subsequent regression analyses. In addition, the measured results within  $\pm 3$  Hz of  
285 the line frequency and its first harmonic (for example, 50 Hz and 100 Hz in Europe or 60 Hz and 120 Hz in  
286 North America) are prone to stochastic noise.<sup>2</sup> Data at these frequencies should be discarded in regression  
287 analyses, or, preferably, not measured. The user can check the EIS plot to spot any dispersed point(s) near  
288 the line frequencies. If there is, just remove these data before regression.

## 289 [H2] ENVIRONMENT CONTROL

290 Many electrochemical parameters have a sensitive dependence on temperature. To ensure reliable  
291 and repeatable measurements, a tight control of the cell temperature is required. Temperature control  
292 may be achieved using a thermal bath for glass cells, a heater-and-fan feedback control for a fuel cells,  
293 and an environmental chamber for batteries. This precaution is especially necessary for measurements at  
294 low frequencies. For low-current measurement, cells must be placed into a Faraday cage to shield the  
295 electrical noise from the environment. The Faraday cage should be connected to the ground to eliminate  
296 the voltage difference between the interior of the cage and the ground reference. Otherwise, this voltage-  
297 difference tends to couple capacitively to the electrodes, leading to only partial shielding of the external  
298 electro-magnetic interference.<sup>69</sup> Mechanical vibration may become an issue for systems with extremely  
299 small current and high sensitivity to electrical contact, such as when probing the EIS of a single particle. In  
300 these situations and those similar, an anti-vibration table should be used.<sup>70</sup>

## 301 [H2] DEBUGGING AND CORRECTION

302 When a doubt arises about the quality of a measurement, debugging tests could be performed on an  
303 electrical circuit that comes with the potentiostat or an electrical circuit with the similar electrical  
304 characteristics as the electrochemical system under study. The use of the appropriate electrical circuit  
305 with known impedance response allows for identifying instrument and wiring artifacts. An oscilloscope,  
306 preferably analog, is extremely helpful in identifying the presence, magnitude, frequency range and the  
307 nature of the electro-magnetic noise. In addition, the nonlinearity can be captured if a significant  
308 component is detected at high multiples of the perturbation frequency. Some EIS instruments have a

309 digital oscilloscope in the menu that should be exploited in the initial phase to determine the appropriate  
310 range of the amplitude of the perturbing signal. Distortions of the expected ellipse in low-frequency  
311 Lissajous plots provide a good indicator for nonlinear response.<sup>67,68</sup> Impedance data can also be evaluated  
312 by regression of a measurement model to determine the stochastic error structure and the frequency  
313 range that is consistent with the Kramers-Kronig relations.<sup>71-73</sup>

## 314 [H1] RESULTS

315 The first step towards data analysis is use of graphical methods to visualize and interpret the  
316 impedance data. To emphasize a specific feature or behaviour, impedance data need to be presented in  
317 different formats that include: the Nyquist representation for mass transfer and kinetic behaviour; the  
318 Bode representation for frequency-dependent behaviour; the admittance format for capacitive behaviour  
319 at high frequency; and the complex-capacitance format for capacitive behaviour of a dielectric system.  
320 The parameters associated with resistance and capacitance can be extrapolated by graphical methods.  
321 Regression and statistical analysis provide more advanced quantitative analysis of impedance data. The  
322 analysis includes checking for consistency with the Kramers-Kronig relations, finding the error structure  
323 of impedance measurements, and extrapolating parameters by regression of process model. The methods  
324 and application to sample data are illustrated in this section.

## 325 [H2] GRAPHICAL REPRESENTATION

326 Interpretation relies partly on data representation, which is a critical aspect in EIS analysis. The  
327 commonly used representations are shown and discussed here.

## 328 [H3] Potential-current vs. time and Lissajous curves

329 The relation of the sinusoidal potential and current as the function of time at a frequency of 20 Hz is  
330 shown in Figure 3a. The amplitude and phase shift contain important information of impedance data. The  
331 phase shift between the input and output signals can be seen more clearly in the Lissajous curve given as  
332 Figure 3b, obtained by plotting the output signal as a function of the input signal at a specific frequency.  
333 In the early years of EIS, Lissajous plots were used to perform EIS measurement at low and high  
334 frequencies, respectively. Moreover, the Lissajous plot (Figure 3b) has several advantages when  
335 monitored during the course of the experiment. If distortions of the Lissajous figure are seen, the  
336 perturbation amplitude applied to the system should be reduced, at least on the frequency domain where  
337 the degeneration of the ellipse is observed. If the Lissajous plot can be made to have an elliptical shape  
338 by adjusting the perturbation amplitude, the measurement can be said to be linear. In addition, a shift of

339 the electrical signal along the x- or y-axis, usually occurring at the low-frequency range, implies a shift of  
340 the system to a non-stationary state, resulting in an erroneous measurement in this frequency domain.  
341 For example, this can be the case for a battery, if the amount of charge changes during the measurement,  
342 or for a corroding system evolving naturally, even slowly, over time. Accordingly, even if the current  
343 measuring devices are becoming more and more efficient, their mode of operation is not generally known  
344 to the user. The recorded current signal, for example, can be an average over a few cycles or a period of  
345 time. Therefore, connecting an **oscilloscope [G]** to trace the live Lissajous curve is a way to guarantee the  
346 validity of the measurements. If the traces of the live Lissajous curves overlap, the measurement at that  
347 frequency is not experiencing non-stationary behaviour, which means the system does not change with  
348 time.

### 349 [H3] BODE AND NYQUIST REPRESENTATIONS

350 The Bode (**Fig. 3c**) and Nyquist (**Fig. 3d**) representations are obtained over a wide frequency range  
351 (typically between 100 kHz and 10 mHz) and are therefore 3D representations of the experimental results,  
352 namely frequency ( $f$ ), modulus ( $|Z|$ ) and phase ( $\phi$ ) for the Bode diagram or frequency, real part ( $Z_r$ )  
353 and imaginary part ( $Z_j$ ) for the Nyquist diagram. The Bode and Nyquist representations are the most  
354 commonly used in the literature, and they generally allow a preliminary analysis of the system, leading to  
355 the identification of elementary processes involved in the mechanism. A typical Bode plot, where the  
356 phase angle ( $\phi$ ) and modulus ( $|Z|$ ) are plotted as a function of frequency, is shown in **Fig. 3c**. The phase  
357 angle and modulus are calculated from the real and imaginary parts from the measurements. The Bode  
358 plot is an intuitive illustration of the impedance change with frequency. The phase angle usually tends  
359 toward  $0^\circ$  at high frequency due to the ohmic resistance of the electrolyte, shown in blue dots in Figure  
360 3(c). The Ohmic-resistance-adjusted phase angle has an asymptotic value of  $-90^\circ$  at high frequency for the  
361 ideally polarizable electrode. If there is a CPE behaviour, the asymptotic value at high frequency would be  
362 lower than  $90^\circ$ . Thus, plots of the ohmic-resistance-adjusted phase angle provide a direct representation  
363 format for a constant-phase element (CPE) behaviour or frequency dispersion behaviour (see **Box 3**). A  
364 typical Nyquist plot, in which the imaginary part is plotted against the real part of impedance data, is  
365 shown in **Fig. 3d**. The Nyquist representation emphasizes larger values of impedance that show the  
366 influence of mass transfer and reaction kinetics. Each symbol is the data point measured at a specific  
367 frequency and the solid dots are used to designate some typical frequencies. In the case for this sample  
368 data, 1.6 kHz is the characteristic frequency for the charge-transfer process of the electrochemical  
369 reaction, which can be used to obtain the characteristic time constant. The low-frequency straight line is

370 the Warburg impedance for mass-transfer process. The time constant is determined by

$$\tau = \frac{1}{2\pi f_c} \quad (5)$$

371 where the time constant is  $\tau = RC_{dl}$  and  $f_c$  is the characteristic relaxation frequency. Several processes  
372 exhibit similar relaxation frequencies, which results in overlapping time constants. However, it is still  
373 possible to distinguish these different time constants using strategies such as regression analysis, the use  
374 of different graphical representations<sup>2,74</sup> or a method based on the distribution function of relaxation  
375 times.<sup>75-77</sup>

### 376 [H3] Other Representations

377 Other methods for representing impedance, such as the complex-admittance format and  
378 complex-capacity format are less used as compared with the representation methods discussed above.  
379 The choice of representation depends on the specific needs for data visualization and interpretation. The  
380 admittance is also a transfer function with real and imaginary parts, which is inversely related to the  
381 impedance. The admittance format emphasizes the capacitive behaviour at high frequencies. It is  
382 commonly used in solid-state systems. The complex-capacitance is defined as

$$C(\omega) = C_r + jC_j = \frac{1}{j\omega(Z - R_e)} \quad (6)$$

383 for an impedance corrected by the ohmic resistance. Like the Nyquist plot, the complex-capacitance  
384 format obscures the frequency dependence of the data. The high-frequency asymptotic value can be used  
385 to determine the capacitance. Therefore, the complex-capacitance format is usually employed to  
386 represent systems for which the capacity is of interest.

### 387 [H3] EIS AND ELECTRICAL CIRCUITS

388 Electrochemical impedance spectra can be represented as a combination of electrical (resistance,  
389 capacitance or inductance) and electrochemical (faradaic) impedances. In particular, thin films on an  
390 electrode surface behave like dielectrics, as does the double layer that forms spontaneously on an  
391 electrified interface. Therefore, electrical circuits are often used to analyze experimental results, but such  
392 an approach masks the physical and chemical properties of the interface.<sup>2,4,13</sup> All Kramers-Kronig-  
393 consistent impedance spectra may be fit by an equivalent circuit, which is the point of using a  
394 measurement model (discussed further in REPRODUCIBILITY AND DATA DEPOSITION). The issue is that  
395 such models are not unique, and fitting by use of an electrical circuit does not necessarily provide useful

396 information concerning the system under investigation. For example, batteries, are most often analyzed  
397 in terms of equivalent electrical circuits because of the complexity of the system;<sup>78</sup> however, mechanistic  
398 models make it possible to take into account all the physical chemistry in an increasingly precise  
399 manner.<sup>79-82</sup>

400 Users often prefer one technique over others, but it is important to note that EIS and other widely  
401 used electrochemical techniques are complementary. For illustration, a system involving reduced species  
402 dissolved in solution (**Fig. 3e**) is presented using CV (**Fig. 3f**), chronoamperometry (**Fig. 3g**), and EIS (**Fig.**  
403 **3h**).

404 The sweep-rate-dependent increase and decrease in value of current with increasing potential in the  
405 CV curves (**Fig. 3f**) reveals the presence of a diffusion-limited system. The difference between the peak  
406 potentials at a given scan rate allows the determination of electron-transfer kinetics. The variations in  
407 peak intensities as a function of the square root of the potential scan rate allows calculation of the  
408 diffusion coefficient.

409 When the same electrochemical system is studied by applying a potential step, little information is  
410 readily apparent from the resulting current as a function of time, shown in **Fig. 3g**. Inflections in the  
411 current response can be seen when time is plotted on a logarithmic scale, shown in the inset for **Fig 3g**,  
412 and these inflections highlight the presence of two time constants. The current response is dominated by  
413 the cell time constant for the shorter times, that is the electrolyte resistance,  $R_e$ , in series with the double  
414 layer capacitance,  $C_{dl}$ . In contrast, the diffusion of electroactive species is responsible for the current  
415 decay for longer times owing to their consumption at the electrode surface. The inset in **Fig. 3g** shows the  
416 current response to the  $R_e C_{dl}$  time constant, characteristic of the double-layer charging. This value  
417 defines the lower limit time scale (2 to 3 times  $R_e C_{dl}$ ) at which kinetic information can be retrieved, and  
418 can be tuned by using an electrode of appropriate size. The use of microelectrodes reduces the ohmic  
419 resistance and so the  $R_e C_{dl}$  time constant (as shown by equation (3)), making it possible to study systems  
420 with fast charge transfer, down to the 100  $\mu$ s domain.<sup>83</sup>

421 Similarly, the detailed analysis of the EIS diagram (**Fig. 3h**) allows these same parameters to be  
422 determined. The width of the high-frequency capacitive loop yields the charge-transfer resistance  
423 associated with the kinetics of the electrochemical reaction, and the frequency at the peak of the high-  
424 frequency loop yields the double-layer capacitance (see equation (5)). The tail forming a 45° slope in the  
425 low-frequency range is attributed to the diffusion of electroactive species (**Warburg semi-infinite diffusion**  
426 **impedance [G]**). Interestingly, the current response to a small-amplitude potential step results in a curve

427 **(Fig. 3g)** that contains the same information as the EIS response, which is enabled by transforming data  
428 from time domain to frequency domain using the Fourier transform.<sup>84,85</sup>

## 429 [H2] REGRESSION

430 Complex nonlinear least-squares regression is used to fit mathematical models to impedance data.  
431 The complex nonlinear least-squares approach has the advantage that a common set of parameters are  
432 obtained by simultaneous regression of the model to both real and imaginary data.<sup>86</sup> Commercial  
433 programs such as ZPlot<sup>87</sup> or ZSimpWin<sup>88</sup> are available to fit electrical circuit models to impedance data.  
434 Noncommercial programs are also available, such as a recent Python-based program for regression that  
435 allows both a measurement-model analysis of the data and the ability to regress arbitrary functions.<sup>73</sup>

436 The quality of the fit may be determined by using a graphical comparison of the model result and the  
437 impedance data or, if the experimental error structure is known, by the weighted-chi-squared statistic.  
438 Both **simplex regression [G]** and **Levenberg-Marquardt regression [G]** strategies are used.<sup>89,90</sup> Despite  
439 being very sensitive to selection of initial guesses, the Levenberg-Marquardt regression method provides  
440 confidence intervals for regressed parameters, thus alerting the user to situations where regressed  
441 parameters do not have statistical significance. The simplex routine is less sensitive to initial guesses and  
442 as a result is easily used, but the absence of confidence intervals represents a severe shortcoming. A  
443 hybrid approach is preferred in which simplex is used to provide good initial guesses for the Levenberg-  
444 Marquardt regression.

## 445 [H2] APPLICATION TO SAMPLE DATA

446 To demonstrate a systematic procedure for interpretation of impedance data, the data analysis  
447 methods discussed above are applied to sample impedance measurements in the following section. The  
448 error analysis associated with these sample data is presented in REPRODUCIBILITY AND DATA  
449 DEPOSITION.

## 450 [H3] SAMPLE DATA

451 The sample data were collected for the impedance response of a 5 mm diameter Pt disk electrode  
452 rotating at 120 rpm in an electrolyte containing 0.01 M  $K_3Fe(CN)_6$ , 0.01 M  $K_4Fe(CN)_6$ , and 1 M KCl as  
453 supporting electrolyte. Overall, this system is widely used as a reference for electrochemical  
454 measurements and further experimental details are available elsewhere.<sup>91</sup> The first frequency  
455 measurement was collected after 14 s, and the subsequent measurements were collected after nine hours  
456 of immersion. Each measurement required about 19.5 minutes for its acquisition. As shown in **Fig. 4a**, a  
457 substantial difference is seen between the first measurement made and the measurements made after

458 8.9 h. A film is hypothesized to form on the platinum disk, and this film is seen to influence the impedance  
 459 results.<sup>91</sup> The regression program used to analyze the data in the present work is available for free non-  
 460 commercial use.<sup>73</sup> The installation file includes all the sample data discussed in this subsection, sample  
 461 process models including the one used to analyze the data, and the Python code used to calculate the  
 462 convective diffusion impedance response of a rotating disk electrode.

### 463 [H3] PROCESS MODEL

464 The depressed high-frequency semicircular loop seen in **Fig. 4a** can be attributed to the faradaic  
 465 reaction and the shape of the larger low-frequency loop, with a 45° line at higher frequencies, can be  
 466 associated with mass transfer. For the ferri/ferro cyanide system, mass transfer is expected to influence  
 467 the faradaic reactions. The depressed character of the high-frequency loop is attributed to frequency  
 468 dispersion that is approximated by a CPE (see **Box 3**). The origin of the observed CPE is uncertain and the  
 469 usual explanations in terms of distributions along the surface of the electrode<sup>92</sup> or through a film<sup>93</sup> are not  
 470 likely to apply. However, the coupling between faradaic and charging current may be a possible reason,<sup>94</sup>  
 471 but more work is needed to explore this hypothesis.

472 The circuit representation of the process model is shown in **Fig. 4b**, and the corresponding  
 473 mathematical expression is given as

$$Z = R_e + \frac{R_t + Z_d}{1 + (j\omega)^\alpha Q(R_t + Z_d)} \quad (7)$$

474 where  $R_e$  is the ohmic resistance,  $R_t$  is the charge-transfer resistance,  $Z_d$  is the diffusion impedance,  
 475 and  $\alpha$  and  $Q$  are parameters for a CPE, that is  $Z_{\text{CPE}} = ((j\omega)^\alpha Q)^{-1}$ . The diffusion impedance is expressed  
 476 in terms of a diffusion resistance  $R_d$  and a dimensionless diffusion impedance as

$$Z_d = R_d \left( \frac{-1}{\theta'(0)} \right) \quad (8)$$

477 The dimensionless diffusion impedance is given by

$$\frac{-1}{\theta'_1(0)} = Z_{(0)} + \frac{Z_{(1)}}{\text{Sc}_i^{1/3}} + \frac{Z_{(2)}}{\text{Sc}_i^{2/3}} + \dots \quad (9)$$

478 where  $Z_{(0)}$ ,  $Z_{(1)}$ , and  $Z_{(2)}$  are the three complex solutions to the convective diffusion impedance  
 479 corresponding to three terms in the series expansion for the axial velocity near the disk electrode, and

480 the Schmidt number is expressed as  $Sc = \nu / D_i$ , where  $\nu = \mu / \rho$  is the kinematic viscosity and  $D_i$  is the  
 481 diffusion coefficient for the reacting species.<sup>2</sup> The dimensionless diffusion impedance for a stationary film  
 482 in terms of a diffusion time constant  $\tau = \delta_{N,i} / D_i$ , where  $\delta_{N,i}$  is the Nernst stagnant diffusion layer  
 483 thickness,

$$\frac{-1}{\theta'_i(0)} = \frac{\tanh \sqrt{j\omega\tau}}{\sqrt{j\omega\tau}} \quad (10)$$

484 is often used to account for the impedance of a rotating disk. The advantage of equation (9) over equation  
 485 (10) is that it provides a more accurate model for the diffusion impedance response of a rotating disk  
 486 electrode with no additional parameters.

### 487 [H3] REGRESSION

488 The regression was weighted by the error structure deduced from the three measurements  
 489 collected after 8.9 hours of immersion, such that

$$\sigma_r = \sigma_j = \beta |Z_r| + \gamma |Z|^2 \quad (11)$$

490 where  $\beta = 0.000291$  and  $\gamma = 3.76 \times 10^{-5} \Omega^{-1} \text{cm}^{-2}$ . Five low-frequency data points were found to be  
 491 inconsistent with the Kramers-Kronig relations and were removed from the first data set (measured at  
 492 14s). No low-frequency data were removed from the data collected after 8.9 hours. Data with frequencies  
 493 above 4.3 kHz were removed to eliminate the contribution of ohmic impedance associated with  
 494 nonuniform current and potential distributions. The resulting regression results are illustrated as lines in  
 495 **Fig. 4a** and the values of the fitted parameters are summarized in **Table 1**, which were all statistically  
 496 significant. The Schmidt number for the measurement at 14 s is  $1076 \pm 14$ , on the order of the value  
 497 expected for a bare electrode under the measurement conditions. There was an observed increase in the  
 498 Schmidt number after 8.9h of immersion. Similarly, the charge-transfer resistance and the diffusion  
 499 resistance increased with elapsed time. The effective capacitance was evaluated based on the values from  
 500 regression results, following the Brug formula,<sup>92</sup>

$$C_{\text{eff}} = Q^{1/\alpha} \left( \frac{R_e R_t}{R_e + R_t} \right)^{(1-\alpha)/\alpha} \quad (12)$$

501 where  $R_e$  is the ohmic resistance.  $R_t$  is the charge-transfer resistance, and  $\alpha$  and  $Q$  are the values  
 502 associated with the CPE. Equation (12) relates the CPE parameters to capacitance for a surface distribution

503 of time constants. The values shown in **Table 1** are in the range expected for a double-layer capacitance.  
504 The characteristic frequencies, calculated using equation (2), are larger than the maximum frequency used  
505 in the regression, confirming that the influence of ohmic impedance was avoided.

506 The analysis presented here demonstrates the discriminating power of impedance spectroscopy.  
507 The method allows an in-situ interrogation of an electrochemical system. The method is noninvasive such  
508 that the potential excursion is very small as compared to CV, and it can be used to evaluate the ohmic  
509 resistance, the electrode capacitance, the charge-transfer resistance, which is inversely related to the  
510 reaction rate constant, and the Schmidt number. The EIS measurement is very sensitive to the evolution  
511 of electrode properties, in this case, showing the influence of the growth of a film on the electrode. The  
512 presence of a film increases the charge-transfer resistance, increases the electrode capacitance, and  
513 influences mass transfer. The systematic changes revealed by the impedance response are not visible in  
514 the steady-state current at the applied potential given in **Table 1**.

## 515 [H1] APPLICATIONS

516 EIS is widely applied across diverse electrochemical cells, devices and systems, including energy  
517 storage and conversion, corrosion, sensors and biomedical systems. This method can be used to provide  
518 simple system diagnostics in-situ and in-operando, to identify the presence and evaluate the relative  
519 importance of different processes or to extract detailed physical and chemical information about a  
520 process of interest.

## 521 [H2] PROCESS DECOUPLING AND DIAGNOSING

522 In the initial stage or pre-test, EIS may be used to probe the general behaviour of the system, similar  
523 to the use of the CV technique in the time domain. In CV, voltage is swept across a wide range (1~2 V) to  
524 expose current peaks corresponding to different electrochemical reactions, in the anodic and cathodic  
525 scans. In EIS, frequency is swept across several orders of magnitude to expose impedance features and  
526 signatures at different time scales. Major features can be easily identified, while abnormal behaviours can  
527 be easily spotted.

528 EIS provides a powerful means for decoupling processes occurring at different time scales as  
529 compared to time-domain methods. The typical EIS spectra and the corresponding physical processes of  
530 iron corrosion in sulfuric acid solution<sup>95</sup>, solid oxide fuel cells<sup>96</sup>, lithium-ion batteries<sup>80</sup> and polymer  
531 electrolyte fuel cells<sup>97</sup> are shown in **Figure 5**. Generally, electrolyte resistance dominates at the high-  
532 frequency range, diffusive impedance dominates at the low-frequency ranges, and interfacial processes

533 dominate at the intermediate-frequency range. Inductive loops are frequently observed, as shown here  
534 for a corrosion process and for a polymer-electrolyte fuel cell. The inductive loops for the corrosion of  
535 iron in sulfuric acid were attributed to the coupling of electrochemical reactions by three intermediate  
536 species.<sup>28,98</sup> Depending on the operating conditions, the inductive loops for the polymer-electrolyte fuel  
537 cell have been attributed to water transport<sup>99</sup>, reactions coupled by oxidation of the Pt catalyst<sup>100</sup> or  
538 adsorbed intermediates (discussed further in LIMITATIONS AND OPTIMIZATIONS).

539 These physical processes can be further decoupled. For example, a physics-based model for lithium-  
540 ion batteries was able to resolve the controversial attribution of EIS features at low frequency to diffusion  
541 in either electrolyte or active particles.<sup>79,80,101</sup> The contributions from different parts in the cell (the anode,  
542 the cathode, the electrolyte) may be differentiated even without the use of a reference electrode.<sup>102,103</sup>  
543 The diagnostic results from EIS can help identify the rate-determining process, and are hence valuable for  
544 the design and evaluation of electrochemical devices.

545

## 546 [H2] MECHANISM IDENTIFICATION AND REACTION PARAMETER ESTIMATION

547 EIS can be employed to identify reaction or failure mechanisms from EIS signatures or the evolution  
548 of EIS features. Once the mechanism is identified, EIS can be employed to estimate the reaction  
549 parameters, such as charge-transfer resistance and the diffusion coefficient. A systematic way to identify  
550 the reaction mechanism composed of different elementary steps has been established, showing that the  
551 development of impedance models from assumed reaction kinetics is superior to the interpretation of  
552 impedance data in terms of an intuitively assumed electrical circuit.<sup>104</sup> One way to validate the proposed  
553 mechanism is to check whether a single set of parameters can describe the current-voltage curve and the  
554 electrochemical impedance measured at different potentials.<sup>28,98,105-107</sup>

555 The underlying mechanism for the deposition of hydrogen under potential was explored using EIS.<sup>108</sup>  
556 Dynamic EIS and dynamic CV were used to resolve the controversy over the failure mechanism during  
557 subzero startup of a proton-exchange membrane fuel cell.<sup>109</sup> The exchange current density, related to the  
558 charge transfer resistance, can be estimated from EIS at the open circuit voltage.<sup>110</sup> The reaction order of  
559 different species can be estimated from the exchange current density at different reactant concentrations  
560 (activities).<sup>111</sup> Finally, the activation energy ( $E_a$ ) can be estimated from the exchange current density at  
561 several reaction temperatures<sup>110,112</sup>, as shown in Error! Reference source not found.6.

562

## [H2] MONITORING

The features in EIS can be attributed to specific components or processes by examining the trend of the impedance data while systematically varying the parameters. The adjusted parameter can be external, such as operation conditions, or internal, such as the cell design parameters. After the EIS features of a system are thoroughly understood, impedance results at several or even a single frequency can be used to monitor the status of the system and subsequently to control the operation condition.

In a proton-exchange membrane fuel cell, impedance at a single frequency (around 1 kHz) is used to monitor the water content of the membrane, based on which the operation conditions are adjusted to prevent both flooding and drying out.<sup>113</sup> In lithium ion batteries, EIS is used to estimate the internal temperature of the cell,<sup>114</sup> which constitutes a more reliable and earlier indicator for possible thermal runaway than the surface temperature. For the online monitoring of EIS, a simplified equivalent electric circuit model, using the general-purpose CPE, usually proves to be adequate. EIS is also widely used for biosensing applications, since it allows the real-time monitoring of tiny changes at the electrode/electrolyte interface.<sup>115-117</sup> For example, EIS methods enabled the detection of breast cancer cell concentration via covalent grafting of the specific antibody directed against the receptor anti c-erbB-2 on electrogenerated polymers (**Fig. 7**).<sup>117</sup> The resistance determined from the zero-frequency limit of the impedance is correlated to the concentration of cancer cells, as shown in **Fig.7**. The impedimetric biosensor can measure the EIS continuously and can monitor the concentration of cancer cells with high sensitivity and efficiency.

## [H2] MATERIAL, STRUCTURE, PROCESS CHARACTERIZATION

Once the frequency response of the system being evaluated is well-understood, EIS can be used to characterize the materials, structures and processes of interest, and extract the associated structural, kinetic and mass transfer parameters. To improve the accuracy, it is advisable to devise simplified systems for such purposes.

For material characterization, it is common practice in the laboratory to use EIS with a four-electrode setup to measure the electrolyte conductivity, be it liquid or solid. The four-electrode configuration was used to explore the solvation/desolvation behaviour of the lithium ion, identifying the desolvation of Li<sup>+</sup> ion as the major contributor to the interfacial resistance in lithium-ion batteries.<sup>118</sup> For structure characterization, an electrochemical porosimeter enabled estimating the pore size distribution in a porous electrode using EIS.<sup>119,120</sup> Different pore size distributions correspond to different CPE behaviour, as shown in **Figure 8**. Also, for process characterization, EIS has been used to estimate the charge and mass transfer

594 properties of a lithium-ion battery component.<sup>121</sup> To improve the power of process differentiation, a  
595 generalized transmission-line model for porous electrodes<sup>80</sup> was developed.

## 596 [H1] REPRODUCIBILITY AND DATA DEPOSITION

597 As EIS measurements are very sensitive to sample preparation and the conditions to which the  
598 electrode has been exposed, the use of data repositories as a means to enhance reproducibility has not  
599 been widely adapted. Although round-robin tests have been attempted,<sup>122</sup> these have shown scattered  
600 results, partly because the protocols used emphasized speed of measurement over data quality. To this  
601 end, impedance measurement and interpretation are considered to be specific to each individual  
602 application.

603 Two types of error structure may be considered for impedance measurements. Sample-to-sample  
604 variability is important for use of impedance data for quality control, such as evaluating the durability of  
605 coatings.<sup>123</sup> A minimum of eight samples has been suggested for the commercial evaluation of the relative  
606 performance of different coatings, and 12-18 samples for assessing properties of an individual coating.  
607 The impedance of these coatings would be evaluated as a function of time under accelerated degradation  
608 protocols to assess film durability.<sup>124</sup>

609 The second type of error structure is that associated with each individual measurement. The error  
610 structure of impedance data may be considered in terms of the residual errors for the regression of a  
611 model to impedance data. The residual errors are expressed as<sup>2</sup>

$$Z - \hat{Z} = \varepsilon_{\text{fit}} + \varepsilon_{\text{stoch}} + \varepsilon_{\text{bias}} \quad (13)$$

612 where  $\varepsilon_{\text{fit}}$  is the contribution to the residual error that can be attributed to the use of an inadequate  
613 model,  $\varepsilon_{\text{stoch}}$  is the contribution due to stochastic errors, and  $\varepsilon_{\text{bias}}$  is the contribution due to bias errors.  
614 The stochastic errors have a mean value equal to zero and can be characterized by a standard deviation.  
615 The bias errors may be considered to be those errors that cause the impedance data to be inconsistent  
616 with the Kramers-Kronig relations. Error structure and sample variability should always be evaluated for  
617 a scientific analysis of impedance data, although it is not yet commonplace.

618 The step-by-step procedure for assessing the error structure of replicated impedance spectra  
619 involves fitting the Voigt measurement model shown in **Fig. 9a** to each impedance measurement using  
620 modulus weighting.<sup>71</sup> The impedance is given by

$$Z = R_0 + \sum_k^K \frac{R_k}{1 + j\omega\tau_k} \quad (14)$$

621 where  $R_0$  is the leading resistance, similar to the ohmic resistance used in equation (7),  $\tau_k = R_k C_k$ ,  $k=1 \dots$   
 622  $K$ , and  $K$  is the number of Voigt elements. The estimate of the standard deviation of the stochastic part  
 623 of the error structure is obtained from the standard deviation of the residual errors for the regression. It  
 624 is important that the fit to each spectrum includes the same number of Voigt elements. The resulting  
 625 standard deviation for the data presented in **Fig. 4a** is presented as  $100 \sigma |Z|^{-1}$  in **Fig. 9b**, where the  
 626 standard deviation for the real part of the impedance is given as circles and the standard deviation for the  
 627 imaginary part of the impedance is given as triangles. The standard deviation is seen to be a small  
 628 percentage of the modulus, ranging from about 0.2% at low frequency to about 0.02% at high frequency.  
 629 This standard deviation  $\sigma$  is the error structure used to weight regressions and must be determined for  
 630 each type of experiment.

631 The application of the Kramers-Kronig integrals to impedance data was considered controversial  
 632 in the late 20<sup>th</sup> century because the integrand included an interpolated function of frequency ranging from  
 633 zero to infinity, requiring extrapolation into the unmeasured frequency domain (see **Box 1**). This objection  
 634 was resolved by the regression of a measurement model to the data. This measurement model (**Fig. 9a**)  
 635 satisfied the Kramers-Kronig relations and was shown to provide a satisfactory fit to the impedance data,  
 636 which supports that data fit by the measurement model could be understood to be consistent with the  
 637 Kramers-Kronig relations.<sup>72</sup> Most vendors of impedance instrumentation provide a regression-based  
 638 assessment of the consistency with the Kramers-Kronig relations that is derived from a linear  
 639 measurement model analysis.<sup>125</sup> The nonlinear Voigt measurement model approach described here has  
 640 greater sensitivity to inconsistency with the Kramers-Kronig relations, making it easier to identify  
 641 frequencies for which a given data set does not satisfy the Kramers-Kronig relations.<sup>126</sup>

## 642 [H1] LIMITATIONS AND OPTIMIZATIONS

643 The set of measured signals in CV and EIS contain the same information, which should be easy to  
 644 deconvolute depending on the physicochemical process and whether CV or EIS is used. Nevertheless, it is  
 645 sometimes difficult to compare results obtained from both techniques. Currently, the evaluation of  
 646 interfacial capacitance from CV and EIS for the case of a non-ideal behaviour,<sup>127-130</sup> which is commonly  
 647 depicted as a CPE, remains an unresolved issue. The CPE is considered to result from a position-dependent  
 648 distribution of a time constant, represented as  $\tau(x) = R(x)C(x)$ ,<sup>134</sup> and is often used in an electrical

649 circuit model to improve the fitting to the impedance data (see **Box 3**). The distribution of time constant  
650 along the surface of the electrode may be caused by the variation in surface distribution of current and  
651 potential due to the electrode geometry. The time constant distribution may also be in the direction  
652 normal to the electrode as a result of a distribution of properties for an oxide or polymeric film. In  
653 principle, the interfacial capacitance obtained by EIS and CV for the same system should be the same, but  
654 that equality has not yet been demonstrated experimentally. Both techniques are in situ and measure a  
655 total current and an averaged potential. However, CV measures the global effective observation of the  
656 CPE behaviour over a broad range of potential; whereas EIS provides a measurement at a specified  
657 potential.

658 Analytical electrochemistry experiments usually employ disk electrodes that are studied by means of  
659 a classical three-electrode potentiostat and a frequency response analyzer for measuring the impedance  
660 response. A three-electrode device enables monitoring the electrochemical processes occurring only at  
661 the working electrode, dissociating them from the processes taking place at the counter-electrode.  
662 However, even with these simple systems, the impedance response is not trivial. The observed EIS  
663 response depends on the electrochemical reactions at the working electrode, the geometry of the cell as  
664 well as the electrode and the electrolyte conductivity, which often results in a non-ideal response of the  
665 interfacial capacitance.<sup>54,131-134</sup> Independent of this frequency dispersion that is ascribed to the cell  
666 geometry and that gives rise to a high-frequency ohmic impedance,<sup>54</sup> the capacitive behaviour of the  
667 interface is rarely ideal and requires the use of a CPE for its description.<sup>93,135,136</sup> Also, commercial reference  
668 electrodes usually have high impedance that leads to high frequency artifacts, but this drawback can be  
669 overcome by using a dual reference electrode.<sup>57</sup> Overall, the measured electrochemical impedance  
670 depends on the mechanism under investigation in addition to the extrinsic parameters that are not  
671 associated with the mechanism, such as the geometry of the cell and the electrode.

672 Some systems are inherently more complex. For example, the study of corrosion<sup>137,138</sup> or corrosion  
673 protection<sup>139,140</sup> systems using coatings have small current densities, and thus require measurements  
674 using large electrodes.<sup>141,142</sup> Measurements on batteries are most often performed on two-electrode  
675 systems. The contributions of both electrodes are then measured simultaneously, which makes the  
676 analysis of the response even more complex because it includes the sum of the positive and negative  
677 electrode contributions. This experimental difficulty can be circumvented by inserting a reference  
678 electrode in the device<sup>46,143,144</sup> or using a symmetric cell.<sup>145,146</sup> Other artifacts may exist, such as an  
679 inductive contribution caused by the connecting wires in the high-frequency domain when low

680 impedances are measured (for batteries applications) or a significant noise in the low-frequency range  
681 when measuring high impedance (for anti-corrosion coatings). In the latter case, a potentiostat that allows  
682 the measurement of small currents must be used and the measurement must be carried out in a Faraday  
683 cage. A simple way to eliminate measurement errors related to the equipment is to perform the same  
684 measurement on an equivalent electrical circuit exhibiting similar characteristics (time constants and  
685 impedance magnitude) as the electrochemical system under study.

686 Different techniques have been developed to perform impedance measurements with respect to  
687 instrumentation, where the most common one is the FRA<sup>4</sup>. However, other approaches such as the use  
688 of multisine,<sup>69,147,148</sup> white noise<sup>149,150</sup> or wavelet<sup>151,152</sup> are also used, but their description is outside the  
689 scope of this Primer. These techniques have also been used to evaluate other transfer functions involving  
690 electrochemical systems such as thermal impedance spectroscopy,<sup>153</sup> electrohydrodynamic impedance<sup>154-</sup>  
691 <sup>156</sup>, modulation of the interfacial capacitance<sup>157-160</sup> and local electrochemical impedance spectroscopy.<sup>161-</sup>  
692 <sup>165</sup>

## 693 [H2] FIELD-SPECIFIC LIMITATIONS

694 A general purpose EIS module may not have adequate accuracy for the test sample one wants to  
695 measure and depending on the application of EIS different issues are likely to arise.

## 696 [H3] LOW-FREQUENCY RANGE

697 For measurement at low frequency, the major problem is the long measurement time and the  
698 drifting or non-stationarity of the system. The lower the frequency, the more pronounced this problem is.  
699 The multi-sine method has been proposed to alleviate the problem by reducing the measurement time,<sup>166</sup>  
700 but the result represents an averaged behaviour that is always consistent with the Kramers-Kronig  
701 relations.<sup>126</sup> Thus, the Kramers-Kronig relations cannot be used to detect the influence of nonstationary  
702 behaviour on multi-sine measurements.

703 In lithium-ion batteries, potentiostatic EIS at low frequency will involve the charging and discharging  
704 of the cell, revealing a capacitive behaviour.<sup>167</sup> For galvanostatic EIS, the cell is under charging or  
705 discharging, hence non-stationary conditions, violating one of the three prerequisites for impedance.  
706 However, continuous efforts to measure the EIS of a non-stationary system, frequently under the rubric  
707 of dynamic EIS, have been reported over the years. Following the first report of studying a non-stationary  
708 system in 1985;<sup>168</sup> a proposed time correction method was used to study rechargeable lithium ion  
709 batteries<sup>169</sup> and criterion for the restriction on the amplitude was explored in a discharging/charging  
710 process.<sup>170</sup>

711 For proton-exchange membrane fuel cells (PEMFCs), additional features appear at low frequencies  
712 with controversial explanations. For example, inductive loops attributed to different mechanisms, such as  
713 humidity dependent ionomer properties,<sup>171</sup> poisoning of Pt oxide growth<sup>172</sup> or relaxation of intermediate  
714 adsorbed species in multi-step ORR reaction, are observed in the low frequency range.<sup>173</sup> However, the  
715 dominant mechanism for these inductive loops may vary with working condition. The lower the humidity,  
716 the more significant the effect of water transport across the membrane; the higher the potential, the  
717 greater the effect of Pt oxide formation and intermediate species adsorption. In a distributed EIS  
718 measurement, local EIS at downstream even ventured into the second quadrant (negative real and  
719 negative imaginary), a peculiar behaviour that is associated with the consumption and interaction of O<sub>2</sub>  
720 along the channel<sup>174</sup>. Dedicated complementary observations are needed to prove or disprove the  
721 proposed mechanisms and the conjecture that the dominant mechanism may vary with working  
722 condition.

### 723 [H3] REFERENCE ELECTRODES

724 Reversible hydrogen electrodes and dynamic hydrogen electrodes<sup>47</sup> are employed as reference  
725 electrodes in PEMFCs. The tip of the reference electrode is usually located outside the active area,<sup>175</sup> due  
726 to the narrow space (~10 μm) between the anode and cathode. In coin cells or pouch-type lithium-ion  
727 batteries, reference electrodes are either placed between the electrodes or outside the active area of the  
728 electrodes.<sup>176</sup> Although artifacts such as current leaking and short circuit have been associated with  
729 placing the lithium metal reference electrode between the two electrodes.<sup>177</sup> For durable use of reference  
730 electrodes in lithium-ion batteries, in-situ electrochemical alloying a thin insulated gold wire with  
731 lithium<sup>178</sup> and plating Li in nickel mesh<sup>179</sup> are a couple of potential routes. Such reference electrodes can  
732 last reliably for months, which is extremely valuable for diagnosing cells under cycling.

### 733 [ H1] OUTLOOK

734 The development of EIS over the past decades has enabled a better understanding of many  
735 electrochemical systems involved in our modern technologies. The versatility of EIS and its ability to  
736 retrieve in situ quantitative information from complex electrochemical systems has made it an essential  
737 and complementary tool for electrochemists. However, careful considerations on the choice of  
738 experimental conditions and appropriate mathematical models that would accurately describe the  
739 physics and reactions mechanisms involved in the system considered are necessary. EIS is used as a  
740 routine tool for electrochemical characterization, however, the analysis is often limited to regression of  
741 equivalent electrical circuits<sup>180</sup>.

742 Since the 1980s, the EIS technique has benefited from substantial advances in electronic  
743 instrumentation that have facilitated impedance measurements. These advances will continue, often with  
744 specific objectives such as enabling measurement of local electrochemical impedance or coupling EIS with  
745 other transfer-function measurements. Different routes can be considered to measure the local  
746 impedance. The use of a bi-electrode allows these measurements, but the spatial resolution is currently  
747 limited to about 1  $\mu\text{m}$ . Optical measurements provide an interesting way to improve this resolution, but  
748 they are limited to an interface whose topography does not change with time, which is thus not suitable  
749 for the study of many systems such as corroding materials or for systems that experience volume changes  
750 as a function of their state of charge such as battery materials. The use of multiple transfer functions  
751 combining the traditional electrochemical measurement with that of one or more other parameters such  
752 as temperature, pressure, or hydrodynamic conditions of the solution is another area of development.

753 The analysis and interpretation of the large quantities of impedance data that can be generated in a  
754 laboratory or industrial setting is another area of interest. Automated circuit modeling of impedance data  
755 has been proposed, but circuit models obscure the underlying physics and chemistry. In particular,  
756 impedance models are not unique and EIS is not a stand-alone technique. Hypothesis-driven models can  
757 guide selection of complementary experiments that can be used to allow the user to gain confidence in  
758 their model or disprove it.

759 Interpretation of impedance measurements requires both a model that accounts for the chemistry  
760 and physics of the system under study and the error structure of the data. The quality of the measurement  
761 may be assessed using various approaches. The stochastic and bias contributions to the error structure  
762 may be identified by use of recently published software.<sup>73</sup> Manufacturers of impedance instrumentation  
763 are urged to include estimates of the standard deviation of impedance measurement as part of their  
764 standard output, and researchers are encouraged to consider sample-to-sample variability when  
765 appropriate. Overall, verifying the consistency of analyzed data with the Kramers-Kronig relations should  
766 become a standard for publication of impedance data.

767 EIS data interpretation will move in two major directions. The first is the rapid automated  
768 interpretation of data, which can be quantitative if driven by a solid understanding of the system under  
769 study, but is otherwise a qualitative assessment. The other direction includes a more systematic analysis  
770 that sees EIS as one of a set of complementary tools that can be used to explore the physics and chemistry  
771 of electrochemical systems.<sup>97</sup> The automated interpretation will facilitate use of impedance for  
772 diagnostics such as understanding the health of batteries in electric vehicles, enhancing signal processing

773 for subcutaneous glucose sensors or for rapid processing of data collected from multichannel test stations.

774 The system-specific modeling will enhance the ability of research labs to understand the broad range of

775 systems for which EIS may be used.

776

## FIGURE CAPTIONS

**Figure 1. Required steps to acquire an electrochemical impedance spectroscopic measurement.** This includes an electrochemical system (a) with a working electrode (WE), a counter electrode (CE), and a reference electrode (RE). In this example, a periodic perturbation signal ( $\Delta E$ ) is applied between WE and RE from high to low frequencies (b), and the electrochemical response to this perturbation is measured in the linear domain (c). Impedance data are often presented in Nyquist or Bode representations (d) and may be represented by an equivalent circuit in which a mechanistic interpretation of the system under study is used to extract a meaning for the faradaic impedance  $Z_f$  (e).

**Figure 2. Guidelines for EIS measurements.** a) Schematic representation of the two-electrode setup. b) Schematic representation of the three-electrode setup; c) schematic representation of the four-electrode setup, where WE is the working electrode, WSE is working sense electrode, RE is the reference electrodes, and CE is the counter electrode. d) Accuracy contour plot in which line A is the maximum measurable impedance, B is the capacitive limit, C is the maximum measurable frequency, D is the inductive limit, and E is the lowest measurable impedance. e) Circuit representation showing the influence of wire capacitance, resistance, and inductance on the measured impedance. For most measurements, the contribution of wire properties can be neglected, and measured impedance is the same as the cell impedance. Acceptable measurements may be made in the region with  $<1\%$  error in magnitude and  $<2^\circ$  error in phase. Measurements in the region marked  $>10\%$ ,  $>10^\circ$  will show anomalous features caused by the instrument and cabling. f) Schematic representation of a wire connection to the electrochemical cell, where  $V_1$  and  $V_2$  are the voltage connectors, and  $A_1$  and  $A_2$  are the current connectors; g) twisted wires suppress mutual induction.

**Figure 3. EIS data of an ideally polarizable electrode obtained for a redox couple in solution.** a) Temporal measurements of potential and current as a function of time at frequency of 20 Hz where the red line is current density and the blue line is potential, b) Lissajous curve (current as function of potential) plotted from the results presented in (a), c) Bode representation - modulus and phase of impedance as a function of the frequency, d) Nyquist representation - imaginary part of impedance as a function of the real part in a complex plane with frequency as a parameter, e) representation of a mass-transfer controlled electrochemical reaction involving an oxidized species Ox and a reduced species Red, f) cyclic voltammetry with scan rate as a parameter, and g) chronoamperometry with time in a linear and logarithmic (inset plot) scale. All these results shown in (f) and (g) were obtained for the same set of parameters for a planar-disk electrode ( $A= 0.2 \text{ cm}^2$ ) under assumption of a Butler-Volmer relationship for a quasi-reversible process with semi-infinite diffusion:  $k^0 = 10^{-2} \text{ cms}^{-1}$ ;  $\alpha = 0.5$ ;  $E^0 = -0.1 \text{ V/NHE}$ ;  $D_{\text{ox}} = D_{\text{red}} = 10^{-5} \text{ cm}^2\text{s}^{-1}$ ;  $C_{\text{ox}}^* = 10 \text{ mM}$ ;  $C_{\text{red}}^* = 0 \text{ mM}$ ;  $R_e = 5 \Omega$ ;  $C_{\text{dl}} = 10 \mu\text{F}$ .

**Figure 4. Sample analysis of impedance data.** a) Impedance data in a Nyquist format for reduction of ferricyanide on a 5 mm diameter Pt disk rotating at 120 rpm after 14 s, 32135 s, 33305 s and 34472 s. The lines represent the weighted fit of equation (7) to the data. The difference between the first measurement (14 s) and measurements taken after 8.93 hours can be attributed to the slow formation of a film on the

817 electrode surface. b) Electrical circuit corresponding to convective diffusion to a rotating disk electrode  
818 with high-frequency CPE behaviour where  $R_e$  is the ohmic resistance,  $R_t$  is the charge-transfer resistance  
819 associated with electrode kinetics,  $a$  and  $Q$  are parameters associated with the CPE, and  $Z_D$  is the  
820 diffusion impedance associated with transport of reactive species to the electrode surface. The graph  
821 generated in panel a uses data reported in reference 91.

822

823 **Figure 5. Typical EIS spectra and the corresponding physical processes.** a) iron corrosion in sulfuric acid  
824 solution,<sup>94</sup> b) solid oxide fuel cells,<sup>95</sup> c) lithium-ion batteries,<sup>79</sup> and d) polymer electrolyte fuel cells. The  
825 circled numbers in Figures 5b, 5c, and 5d refer to transport and reaction mechanisms and their influence  
826 on the respective Nyquist plots. Panel a is adapted with permission from ref 94, IOP. Panel b is adapted  
827 with permission from ref 95, RSC. Panel c is adapted with permission from ref 79, IOP.

828

829 **Figure 6. The use of EIS measurements at different temperatures to extract activation energy.** a) The  
830 current-overpotential curve for electrochemical systems showing the relationship between exchange  
831 current to the slope of the current-potential plot and b) the activation energy is obtained from the slope  
832 of the exchange current density as a function of inverse absolute temperature. The charge-transfer  
833 resistance is obtained from the high-frequency loop of the inset impedance diagram.<sup>110</sup> Panels a and b  
834 adapted with permission from ref 109, Elsevier.

835 **Figure 7. Use of EIS to detect the concentration of breast cancer cells.** This was achieved via covalent  
836 grafting of the specific antibody directed against the receptor anti c-erbB-2 on electrogenerated polymers:  
837 a) EIS of system with MCF-7 cancer cells<sup>116</sup> where (1) 0 cell/mL, (2) 100 cell/mL, (3) 1000 cell/mL, (4) 10000  
838 cell/mL, (5) 100000 cell/mL and b) evolution of the resistance change as compared to case i,  $\Delta R_z$ , as  
839 a function of the concentration of MCF-7 cancer cell. Error bars show the relative standard deviation  
840 (RSD=5%) of three identical experiments. Panels a and b adapted with permission from ref 116, Elsevier.

841

842 **Figure 8. Influence of pore size distribution on impedance behavior.** a) Impedance of porous materials  
843 with various pore size distributions,<sup>119,120</sup> where  $R_{pore}$  is the pore resistance, and b) corresponding pore  
844 size distribution of porous materials where  $\bar{r}$  is the average radius and  $\sigma$  is the standard deviation of the  
845 radius distribution. Panels a and b adapted with permission from ref 119, Elsevier.

846

847 **Figure 9. Measurement model analysis to identify the error structure of impedance data.** a) Schematic  
848 representation of a Voigt circuit used as a measurement model.<sup>181</sup> To improve the stability of the  
849 regressions, the model, as shown in equation (14), is written in terms of resistors and time constants.  
850 Taken from Liao, et al.<sup>182</sup> The Voigt measurement model may be used to assess the error structure of  
851 impedance measurements and to provide preliminary physical properties such as ohmic resistance and  
852 capacitance. b) The standard deviation of the stochastic part of the error structure for the data presented  
853 in Figure 7. The measurement model approach was used to filter lack of replication in repeated  
854 measurements. Panel a adapted with permission from ref 181, Elsevier.

## TABLES

**Table 1:** Results from the weighted regression of equation (7) to the sample data presented in **Fig. 7**. Confidence intervals given are  $\pm 1\sigma$ . The  $\chi^2/\nu$  statistic should be on the order of unity for a perfect regression. These results show that the model could be further improved. The effective capacitance and characteristic frequency were calculated from the regressed parameters. The current and potential were measured after each EIS measurement.

Parameters (units)	14 s	32135 s	33305 s	34472 s
<b>Sc</b>	1076±14	1235.7±7.8	1244.8±8.0	1256.5±8.3
<b>R<sub>e</sub> (Ω cm<sup>2</sup>)</b>	1.252±0.072	1.381±0.011	1.383±0.011	1.382±0.011
<b>Q (μF s<sup>α-1</sup> cm<sup>-2</sup>)</b>	460±68	59.8±1.2	59.4±1.2	59.6±1.3
<b>R<sub>d</sub> (Ω cm<sup>2</sup>)</b>	31.719±0.066	33.199±0.031	33.289±0.032	33.390±0.033
<b>R<sub>t</sub> (Ω cm<sup>2</sup>)</b>	1.273±0.078	3.137±0.013	3.161±0.013	3.188±0.013
<b>α</b>	0.702±0.026	0.9048±0.0.0028	0.9057±0.0.0028	0.9052±0.0.0029
<b>χ<sup>2</sup>(ν)</b>	139	53	56	59
<b>C (μF cm<sup>-2</sup>)</b>	14.4	21.4	21.5	21.4
<b>f<sub>c</sub> (kHz)</b>	8.8	5.4	5.4	5.4
<b>Current (mA)</b>	90.3	91.3	91.3	90.2
<b>Potential(mV)</b>	215.6	215.7	215.7	215.7

857 BOXES

858 [BH1] BOX 1. KRAMERS KRONIG TRANSFORMATIONS

859

860 The Kramers-Kronig transformations were derived under the assumptions that a system is: stable such  
861 that perturbations to the system do not grow; responds linearly to a perturbation; and is causal where a  
862 response to a perturbation cannot precede the perturbation. These relations are widely used as part of a  
863 validation procedure to identify the frequency ranges that may have been corrupted by instrument  
864 artifacts or by nonstationary behavior.

865 The imaginary part of the impedance can be calculated from the real part through:

866 
$$Z_j(\omega) = -\frac{2\omega}{\pi} \int_0^{\infty} \frac{Z_r(x) - Z_r(\omega)}{x^2 - \omega^2} dx$$

867 If the high-frequency limit of the impedance is known ( $Z_r(\infty)$ ), the real part can be obtained from the  
868 imaginary part through:

869 
$$Z_r(\omega) = Z_r(\infty) + \frac{2}{\pi} \int_0^{\infty} \frac{xZ_j(x) - \omega Z_j(\omega)}{x^2 - \omega^2} dx$$

870 Direct integration of the Kramers-Kronig relations for EIS measurements has been replaced, in modern  
871 use, by regression of Kramers-Kronig-consistent circuit models that provide extrapolation to zero and  
872 infinite frequency limits that is consistent with the behavior of electrochemical systems.

873

874 [BH1] BOX 2. LINEARITY, STABILITY AND CAUSALITY

875 [BH2] LINEARITY

876 The constraint of linearity means that the response to an input perturbation is a linear function of the  
877 single- or multi-frequency input. Because the current is a nonlinear function of potential for  
878 electrochemical systems, linearity is achieved by using a small input perturbation such that the current  
879 can be expressed by the first term of its Taylor series expansion. The choice of an input perturbation  
880 magnitude is a compromise between the need to achieve linearity and the need for a sufficient signal-to-  
881 noise ratio.

882 [BH2] STABILITY

883 The constraint of stability means that the response to a perturbation cannot grow with time. The current  
884 response to a step in potential must eventually decay to a new steady value.

885 [BH2] CAUSALITY

886 The constraint of causality means that the response to a perturbation cannot precede the perturbation.  
887 This constraint ensures that the measured AC-response of the system to an external modulation must be  
888 correlated only to the applied AC perturbation. Causality is especially important for electrochemical  
889 systems because measurements can take minutes to hours, depending on the frequency range used, and  
890 non-stationary behavior leads to failure of causality.

891

892 [BH1] BOX 3. CONSTANT-PHASE ELEMENT (CPE)

893 The CPE is often used to improve the fit of models to impedance data. The CPE parameters  $\alpha$  and  $Q$  cannot  
894 be used directly to extract a capacitance; however, a capacitance may be extracted under assumption of  
895 a distribution of time constants along the electrode surface or through a film. Not all time-constant  
896 distributions give rise to a CPE. The ohmic-resistance-corrected phase angle provides a convenient way to  
897 determine if a time-constant distribution is represented by a CPE.

898

899 GLOSSARY

900 Capacitance: the ability of the electrochemical system, specifically the electrode-electrolyte interface, to  
901 hold electrical charge. ( $F\ m^{-2}$ )

902 Chronoamperometry: Electrochemical technique in which a potential step is applied to a working  
903 electrode and the current response is recorded as a function of time.

904 Chronopotentiometry: Electrochemical technique in which a current step is applied to a working  
905 electrode and the potential response is recorded as a function of time.

906 Complex number: ordered pair of real and imaginary numbers.

907 Cyclic voltammetry: Electrochemical technique in which the current response of an electrochemical  
908 system is measured as a function of the potential, which is swept in positive and negative directions at a  
909 given rate.

910 Frequency decade: a unit for measuring frequency ratios on a logarithmic scale, with one decade  
911 corresponding to a ratio of 10 between two frequencies (an order of magnitude difference).

912 Interfacial capacitance: capacity of the electrical double layer or the double layer in series with a thin  
913 film on the electrode surface. ( $F\ m^{-2}$ )

914 Levenberg-Marquardt regression: a mathematical algorithm used to solve non-linear least squares  
915 curve-fitting problems that is sensitive to initial values and provides confidence intervals for the  
916 resulting parameter estimates.

917 Ohmic resistance: an ionic resistance of the electrolyte and electronic resistance of the electrode, wire  
918 and connection ( $\Omega\ m^2$ )

919 Oscilloscope: an electronic hardware monitoring the time-domain signals that are processed in the  
920 impedance measurement (for example, Lissajous plot).

921 Potentiostat: electronic hardware for electrochemical experiments maintaining a constant potential  
922 difference between the working electrode and the reference electrode.

923 Reactance: imaginary part of the impedance of an electrical circuit ( $\Omega\ m^2$ )

924 Resistance: real part of the impedance of an electrical circuit ( $\Omega\ m^2$ )

925 Rotating Disk Electrode: setup allowing the control of the rotation rate of a disk electrode embedded in  
926 an insulating circular plane in order to enhance and tune mass transport by generating a thin diffusion  
927 layer with uniform thickness.

928 Scanning electrochemical microscopy: local electrochemical technique that allows for sensing the  
929 surface topography and reactivity

930 Simplex regression: a robust mathematical algorithm used to solve non-linear least squares curve-fitting  
931 problems that is less sensitive to initial values but does not provide confidence intervals for the resulting  
932 parameter estimates.

933 Warburg semi-infinite diffusion impedance: an impedance element describing the diffusion behaviour of  
934 the electrolyte in the absence of convection with a diffusion layer that can spread to the infinity.

935

936

## REFERENCES

937

- 938 1 Bard, A. J. & Faulkner, L. R. *Electrochemical Methods: Fundamentals and Applications*. Second  
939 edn, (John Wiley & Sons 2001).
- 940 2 Orazem, M. E. & Tribollet, B. *Electrochemical Impedance Spectroscopy*. Second edn, (Wiley,  
941 2017).
- 942 **A good introduction to hypothesis-driven modeling of impedance spectroscopy.**
- 943 3 Macdonald, D. D. *Transient Techniques in Electrochemistry*. (Plenum Press, 1977).
- 944 4 Gabrielli, C. *Identification of electrochemical process by frequency response analysis*. (The  
945 Solartron Ictronic Group 1980).
- 946 5 Barsoukov, E. & Macdonald, J. R. *Impedance Spectroscopy: Theory, Experiment, and*  
947 *Applications*. Second edn, (John Wiley & Sons, 2005).
- 948 6 Deleebeeck, L. & Veltze, S. Electrochemical impedance spectroscopy study of commercial Li-ion  
949 phosphate batteries: A metrology perspective. *Int J Energ Res* **44**, 7158-7182,  
950 doi:10.1002/er.5350 (2020).
- 951 7 Bredar, A. R. C., Chown, A. L., Burton, A. R. & Farnum, B. H. Electrochemical Impedance  
952 Spectroscopy of Metal Oxide Electrodes for Energy Applications. *Acs Appl Energ Mater* **3**, 66-98,  
953 doi:10.1021/acsaem.9b01965 (2020).
- 954 8 Xu, Y. *et al.* A review of impedance measurements of whole cells. *Biosensors and Bioelectronics*  
955 **77**, 824-836, doi:10.1016/j.bios.2015.10.027 (2016).
- 956 9 Bahadir, E. B. & Sezgentürk, M. K. A review on impedimetric biosensors. *Artificial Cells,*  
957 *Nanomedicine and Biotechnology* **44**, 248-262, doi:10.3109/21691401.2014.942456 (2016).
- 958 10 Bandarenka, A. S. Exploring the interfaces between metal electrodes and aqueous electrolytes  
959 with electrochemical impedance spectroscopy. *Analyst* **138**, 5540-5554,  
960 doi:10.1039/c3an00791j (2013).
- 961 11 Sacco, A. Electrochemical impedance spectroscopy: Fundamentals and application in dye-  
962 sensitized solar cells. *Renewable and Sustainable Energy Reviews* **79**, 814-829,  
963 doi:10.1016/j.rser.2017.05.159 (2017).
- 964 12 Margarit-Mattos, I. C. P. EIS and organic coatings performance: Revisiting some key points.  
965 *Electrochim. Acta* **354**, 136725, doi:10.1016/j.electacta.2020.136725 (2020).
- 966 13 Macdonald, D. D. Reflections on the history of electrochemical impedance spectroscopy.  
967 *Electrochim Acta* **51**, 1376-1388 (2006).
- 968 14 Gabrielli, C. Once upon a time there was EIS. *Electrochim. Acta* **331**, 135324,  
969 doi:10.1016/j.electacta.2019.135324 (2020).
- 970 **A detailed description of the EIS history, especially the evolution of EIS measurement**  
971 **equipment.**
- 972 15 Kohlrausch, F. & Nippoldt, W. A. Ueber die Gültigkeit der Ohm'schen Gesetze für Elektrolyte und  
973 eine numerische Bestimmung des Leitungswiderstandes der verdünnten Schwefelsäure durch  
974 alternirende Ströme. *Annalen der Physik* **214**, 280-298, doi:10.1002/andp.18692141006 (1869).
- 975 16 Kohlrausch, F. Ueber die elektromotorische Kraft sehr dünner Gasschichten auf Metallplatten.  
976 *Annalen der Physik* **224**, 143-154, doi:10.1002/andp.18732240110 (1873).
- 977 17 Wien, M. Ueber die Polarisation bei Wechselstrom. *Annalen der Physik* **294**, 37-72,  
978 doi:10.1002/andp.18962940504 (1896).
- 979 18 Warburg, E. Ueber die Polarisationscapacität des Platins. *Ann. Phys.-Berlin* **311**, 125-135,  
980 doi:10.1002/andp.19013110910 (1901).

- 981 19 Hickling, A. Studies in electrode polarisation. Part IV.—The automatic control of the potential of  
982 a working electrode. *Transactions of the Faraday Society* **38**, 27-33, doi:10.1039/TF9423800027  
983 (1942).
- 984 20 Koutecky, J. & Levich, V. G. The use of a rotating disk electrode in the study of electrochemical  
985 kinetics and electrolytic processes. *Zh. Fiz. Khim.* **32**, 1565-1575 (1958).
- 986 21 de Levie, R. On porous electrodes in electrolyte solutions: I. Capacitance effects. *Electrochim.*  
987 *Acta* **8**, 751-780, doi:[https://doi.org/10.1016/0013-4686\(63\)80042-0](https://doi.org/10.1016/0013-4686(63)80042-0) (1963).
- 988 22 de Levie, R. On porous electrodes in electrolyte solutions—IV. *Electrochim. Acta* **9**, 1231-1245,  
989 doi:10.1016/0013-4686(64)85015-5 (1964).
- 990 23 Gerischer, H. & Mehl, W. Zum Mechanismus der kathodischen Wasserstoffabscheidung an  
991 Quecksilber, Silber und Kupfer. *Zeitschrift für Elektrochemie, Berichte der Bunsengesellschaft für*  
992 *physikalische Chemie* **59**, 1049-1059, doi:10.1002/bbpc.19550591031 (1955).
- 993 24 Gerischer, H. Intermediates in electrochemical reactions. *Faraday Discussions of the Chemical*  
994 *Society* **56**, 7-15, doi:10.1039/dc9735600007 (1973).
- 995 25 Klahr, B., Gimenez, S., Fabregat-Santiago, F., Hamann, T. & Bisquert, J. Water oxidation at  
996 hematite photoelectrodes: the role of surface states. *J. Am. Chem. Soc.* **134**, 4294-4302,  
997 doi:10.1021/ja210755h (2012).
- 998 26 Wang, H., Guerrero, A., Bou, A., Al-Mayouf, A. M. & Bisquert, J. Kinetic and material properties  
999 of interfaces governing slow response and long timescale phenomena in perovskite solar cells.  
1000 *Energy & Environmental Science* **12**, 2054-2079, doi:10.1039/c9ee00802k (2019).
- 1001 **A comprehensive review on perovskite solar cells, with emphasis on the use of impedance**  
1002 **spectroscopy for studying kinetics of bulk and interface processes.**
- 1003 27 Epelboin, I., Gabrielli, C., Keddam, M. & Takenouti, H. Model of the anodic behavior of iron in  
1004 sulfuric acid medium. *Electrochim. Acta* **20**, 913-916, doi:10.1016/0013-4686(75)87017-4 (1975).
- 1005 28 Keddam, M., Mattos, O. R. & Takenouti, H. Reaction model for iron dissolution studied by  
1006 electrode impedance. I. Experimental results and reaction model. *J. Electrochem. Soc.* **128**, 257-  
1007 266, doi:10.1149/1.2127401 (1981).
- 1008 **A detailed description of the procedure to follow for EIS interpretation in the case of complex**  
1009 **mechanisms using iron dissolution as an example.**
- 1010 29 Baril, G. *et al.* An impedance investigation of the mechanism of pure magnesium corrosion in  
1011 sodium sulfate solutions. *Journal of the Electrochemical Society* **154**, C108-C113 (2007).
- 1012 30 Gomes, M. P. *et al.* On the corrosion mechanism of Mg investigated by electrochemical  
1013 impedance spectroscopy. *Electrochim. Acta* **306**, 61-70, doi:10.1016/j.electacta.2019.03.080  
1014 (2019).
- 1015 31 de Levie, R. in *Advances in Electrochemistry and Electrochemical Engineering*, 6 329-397 (Eds  
1016 P. Delahay, Ch.W. Tobias - Wiley New York, 1967).
- 1017 **The pioneering work in developing EIS model for porous electrode.**
- 1018 32 Lasia, A. in *Electrochemical Impedance Spectroscopy and its Applications* 1-367 (Springer New  
1019 York, 2014).
- 1020 33 Lasia, A. Impedance of porous electrodes. *J. Electroanal. Chem.* **397**, 27-33, doi:10.1016/0022-  
1021 0728(95)04177-5 (1995).
- 1022 34 Barcia, O. E. *et al.* Further to the paper “Application of the impedance model of de Levie for the  
1023 characterization of porous electrodes” by Barcia *et al.* [*Electrochim. Acta* 47 (2002) 2109].  
1024 *Electrochim. Acta* **51**, 2096-2097, doi:10.1016/j.electacta.2005.06.035 (2006).
- 1025 35 Orazem, M. E. & Tribollet, B. A tutorial on electrochemical impedance spectroscopy. *ChemTexts*  
1026 **6**, 12, doi:10.1007/s40828-020-0110-7 (2020).
- 1027 36 Savéant, J. M. *Elements of Molecular and Biomolecular Electrochemistry: An Electrochemical*  
1028 *Approach to Electron Transfer Chemistry.* (2006).

- 1029 37 Costentin, C., Drouet, S., Robert, M. & Saveant, J. M. A Local Proton Source Enhances CO<sub>2</sub>  
1030 Electroreduction to CO by a Molecular Fe Catalyst. *Science* **338**, 90-94 (2012).
- 1031 38 Oleinick, A., Svir, I. & Amatore, C. A few key theoretical issues of importance in modern  
1032 molecular electrochemistry. *Current Opinion in Electrochemistry* **13**, 33-39,  
1033 doi:10.1016/j.coelec.2018.10.008 (2019).
- 1034 39 Manbeck, G. F., Fujita, E. & Concepcion, J. J. Proton-Coupled Electron Transfer in a Strongly  
1035 Coupled Photosystem II-Inspired Chromophore-Imidazole-Phenol Complex: Stepwise Oxidation  
1036 and Concerted Reduction. *J. Am. Chem. Soc.* **138**, 11536-11549, doi:10.1021/jacs.6b03506  
1037 (2016).
- 1038 40 Garreau, D., Saveant, J. M. & Tessier, D. Potential Dependence of the Electrochemical Transfer-  
1039 Coefficient - Impedance Study of the Reduction of Aromatic-Compounds. *J. Phys. Chem.* **83**,  
1040 3003-3007 (1979).
- 1041 41 Saveant, J. M. & Tessier, D. Variation of the Electrochemical Transfer-Coefficient with Potential.  
1042 *Faraday Discussions* **74**, 57-72, doi:10.1039/dc9827400057 (1982).
- 1043 42 Corrigan, D. A. & Evans, D. H. Cyclic voltammetric study of tert-nitrobutane reduction in  
1044 acetonitrile at mercury and platinum electrodes: Observation of a potential dependent  
1045 electrochemical transfer coefficient and the influence of the electrolyte cation on the rate  
1046 constant. *J. Electroanal. Chem.* **106**, 287-304, doi:[https://doi.org/10.1016/S0022-  
1047 0728\(80\)80175-6](https://doi.org/10.1016/S0022-0728(80)80175-6) (1980).
- 1048 43 Sluyters-Rehbach, M. Impedances of electrochemical systems: Terminology, nomenclature and  
1049 representation - Part I: Cells with metal electrodes and liquid solutions (IUPAC  
1050 Recommendations 1994). *Pure and Applied Chemistry* **66**, 1831-1891,  
1051 doi:doi:10.1351/pac199466091831 (1994).
- 1052 44 Newman, J. S. & Thomas-Alyea, K. E. *Electrochemical Systems*. third edn, 647 (John Wiley &  
1053 Sons, 2004).
- 1054 45 Bockris, J. O. M., Reddy, A. K. N. & Gamboa-Aldeco, M. *Modern Electrochemistry: Electrodicts*.  
1055 second edn, Vol. 2A 764 (Kluwer Academic Publishers, 2000).
- 1056 46 Talaie, E. *et al.* Methods and protocols for electrochemical energy storage materials research.  
1057 *Chemistry of Materials* **29**, 90-105, doi:10.1021/acs.chemmater.6b02726 (2017).
- 1058 47 Bard, A. J., Inzelt, G. & Scholz, F. *Electrochemical dictionary*. (Springer Science & Business Media,  
1059 2008).
- 1060 48 Song, J. Y., Lee, H. H., Wang, Y. Y. & Wan, C. C. Two- and three-electrode impedance  
1061 spectroscopy of lithium-ion batteries. *J. Power Sources* **111**, 255-267, doi:10.1016/s0378-  
1062 7753(02)00310-5 (2002).
- 1063 49 Engebretsen, E. *et al.* Localised electrochemical impedance measurements of a polymer  
1064 electrolyte fuel cell using a reference electrode array to give cathode-specific measurements  
1065 and examine membrane hydration dynamics. *J. Power Sources* **382**, 38-44,  
1066 doi:10.1016/j.jpowsour.2018.02.022 (2018).
- 1067 50 Sone, Y., Ekdunge, P. & Simonsson, D. Proton conductivity of Nafion 117 as measured by a four-  
1068 electrode AC impedance method. *J. Electrochem. Soc.* **143**, 1254-1259, doi:10.1149/1.1836625  
1069 (1996).
- 1070 51 Deslouis, C., Musiani, M. M. & Tribollet, B. Free-standing membranes for the study of  
1071 electrochemical reactions occurring at conducting polymer/electrolyte interfaces. *J. Phys. Chem.*  
1072 **100**, 8994-8999 (1996).
- 1073 52 Keddiam, M., Novoa, X. R. & Vivier, V. The concept of floating electrode for contact-less  
1074 electrochemical measurements: Application to reinforcing steel-bar corrosion in concrete.  
1075 *Corros. Sci.* **51**, 1795-1801, doi:10.1016/j.corsci.2009.05.006 (2009).

- 1076 53 Samec, Z. Electrochemistry at the interface between two immiscible electrolyte solutions (IUPAC  
1077 technical report). *Pure and Applied Chemistry* **76**, 2147-2180, doi:10.1351/pac200476122147  
1078 (2004).
- 1079 54 Huang, V. M.-W., Vivier, V., Orazem, M. E., Pebere, N. & Tribollet, B. The apparent constant-  
1080 phase-element behavior of an ideally polarized blocking electrode a global and local impedance  
1081 analysis. *J. Electrochem. Soc.* **154**, C81-C88 (2007).
- 1082 55 Shchukin, E., Vidensky, I. & Petrova, I. J. J. o. m. s. Luggin's capillary in studying the effect of  
1083 electrochemical reaction on mechanical properties of solid surfaces. **30**, 3111-3114 (1995).
- 1084 56 Newman, J. S. Resistance for Flow of Current to a Disk. *J. Electrochem. Soc.* **113**, 501-502 (1966).
- 1085 57 Tran, A. T., Huet, F., Ngo, K. & Rousseau, P. Artefacts in electrochemical impedance  
1086 measurement in electrolytic solutions due to the reference electrode. *Electrochim. Acta* **56**,  
1087 8034-8039, doi:10.1016/j.electacta.2010.12.088 (2011).
- 1088 **A key paper on the way to circumvent the artefact linked to the reference electrode in the**  
1089 **high frequency mode.**
- 1090 58 Hills, G. & Payne, R. Improved method for measuring the double layer capacity at a dropping  
1091 mercury electrode. Application to measurements at high pressure. *Trans. Faraday Soc.* **61**, 316-  
1092 325 (1965).
- 1093 59 Primer-EG, G, E. & Lock-In, G.-A. (Princeton, 1986).
- 1094 60 Wellstead, P. *Frequency response analysis*. (Solartron Instruments, 1983).
- 1095 61 Pilla, A. A. A Transient Impedance Technique for the Study of Electrode Kinetics: Application to  
1096 Potentiostatic Methods. *J. Electrochem. Soc.* **117**, 467, doi:10.1149/1.2407544 (1970).
- 1097 62 Itagaki, M., Ueno, M., Hoshi, Y. & Shitanda, I. Simultaneous Determination of Electrochemical  
1098 Impedance of Lithium-ion Rechargeable Batteries with Measurement of Charge-discharge  
1099 Curves by Wavelet Transformation. *Electrochim Acta* **235**, 384-389,  
1100 doi:10.1016/j.electacta.2017.03.077 (2017).
- 1101 63 instruments, G. *Accuracy Contour Plots – Measurement and Discussion*,  
1102 <[https://www.gamry.com/application-notes/EIS/accuracy-contour-plots-measurement-and-](https://www.gamry.com/application-notes/EIS/accuracy-contour-plots-measurement-and-discussion/)  
1103 [discussion/](https://www.gamry.com/application-notes/EIS/accuracy-contour-plots-measurement-and-discussion/)> (2020).
- 1104 64 Zhong, G., Koh, C. K., Roy, K., Ieee & Ieee. *A twisted-bundle layout structure for minimizing*  
1105 *inductive coupling noise*. (Ieee, 2000).
- 1106 65 Wojcik, P. T., Agarwal, P. & Orazem, M. E. A method for maintaining a constant potential  
1107 variation during galvanostatic regulation of electrochemical impedance measurements.  
1108 *Electrochim. Acta* **41**, 977-983 (1996).
- 1109 66 Wojcik, P. T. & Orazem, M. E. Variable-amplitude galvanostatically modulated impedance  
1110 spectroscopy as a tool for assessing reactivity at the corrosion potential without distorting  
1111 temporal evolution of the system. *Corrosion* **54**, 289-298, doi:10.5006/1.3284855 (1998).
- 1112 67 Hirschorn, B., Tribollet, B. & Orazem, M. E. On Selection of the Perturbation Amplitude Required  
1113 to Avoid Nonlinear Effects in Impedance Measurements. *Israel Journal of Chemistry* **48**, 133-142,  
1114 doi:10.1560/Ijc.48.3-4.133 (2008).
- 1115 68 Hirschorn, B. & Orazem, M. E. On the Sensitivity of the Kramers-Kronig Relations to Nonlinear  
1116 Effects in Impedance Measurements. *J. Electrochem. Soc.* **156**, C345-C351,  
1117 doi:10.1149/1.3190160 (2009).
- 1118 69 Van Ingelgem, Y., Tourwé, E., Blajiev, O., Pintelon, R. & Hubin, A. Advantages of odd random  
1119 phase multisine electrochemical impedance measurements. *Electroanalysis* **21**, 730-739,  
1120 doi:10.1002/elan.200804471 (2009).
- 1121 70 Dokko, K. *et al.* Kinetic characterization of single particles of LiCoO<sub>2</sub> by AC impedance and  
1122 potential step methods. *J. Electrochem. Soc.* **148**, A422 (2001).

- 1123 71 Agarwal, P., Crisalle, O. D., Orazem, M. E. & Garcia-Rubio, L. H. Application of measurement  
1124 models to impedance spectroscopy. II. Determination of the stochastic contribution to the error  
1125 structure. *J. Electrochem. Soc.* **142**, 4149-4158 (1995).
- 1126 72 Agarwal, P., Orazem, M. E. & Garcia-Rubio, L. H. Application of measurement models to  
1127 impedance spectroscopy. III. Evaluation of consistency with the Kramers-Kronig relations. *J.*  
1128 *Electrochem. Soc.* **142**, 4159-4168 (1995).
- 1129 **An introduction to the use of Voigt measurement models to assess the consistency of**  
1130 **impedance data to the Kramers-Kronig relations.**
- 1131 73 Watson, W. & Orazem, M. E. Measurement Model Program. *ECSArXiv*,  
1132 doi:<https://doi.org/10.1149/osf.io/kze9x> (2020).
- 1133 74 Orazem, M. E., Pebere, N. & Tribollet, B. Enhanced Graphical Representation of Electrochemical  
1134 Impedance Data. *Journal of the Electrochemical Society* **153**, B129-B136 (2006).
- 1135 75 Ivers-Tiffée, E. & Weber, A. Evaluation of electrochemical impedance spectra by the distribution  
1136 of relaxation times. *Journal of the Ceramic Society of Japan* **125**, 193-201,  
1137 doi:10.2109/jcersj2.16267 (2017).
- 1138 **A significant contribution showing the interest of using the distribution function of relaxation**  
1139 **times to identify the different time-constant of an EIS spectra.**
- 1140 76 Wan, T. H., Saccoccio, M., Chen, C. & Ciucci, F. Influence of the Discretization Methods on the  
1141 Distribution of Relaxation Times Deconvolution: Implementing Radial Basis Functions with  
1142 DRTtools. *Electrochim Acta* **184**, 483-499, doi:10.1016/j.electacta.2015.09.097 (2015).
- 1143 77 Dierickx, S., Weber, A. & Ivers-Tiffée, E. How the distribution of relaxation times enhances  
1144 complex equivalent circuit models for fuel cells. *Electrochim. Acta* **355**, 136764,  
1145 doi:10.1016/j.electacta.2020.136764 (2020).
- 1146 78 Nara, H., Yokoshima, T. & Osaka, T. Technology of electrochemical impedance spectroscopy for  
1147 an energy-sustainable society. *Curr Opin Electroche* **20**, 66-77, doi:10.1016/j.coelec.2020.02.026  
1148 (2020).
- 1149 79 Huang, J., Li, Z., Ge, H. & Zhang, J. Analytical Solution to the Impedance of Electrode/Electrolyte  
1150 Interface in Lithium-Ion Batteries. *J. Electrochem. Soc.* **162**, A7037-A7048,  
1151 doi:10.1149/2.0081513jes (2015).
- 1152 80 Huang, J. & Zhang, J. Theory of Impedance Response of Porous Electrodes: Simplifications,  
1153 Inhomogeneities, Non-Stationarities and Applications. *J. Electrochem. Soc.* **163**, A1983-A2000,  
1154 doi:10.1149/2.0901609jes (2016).
- 1155 **A general framework of EIS models that can be applicable to the porous electrodes in LIB, fuel**  
1156 **cell and capacitor.**
- 1157 81 Fuller, T. F., Doyle, M. & Newman, J. Simulation and Optimization of the Dual Lithium Ion  
1158 Insertion Cell. *Journal of The Electrochemical Society* **141**, 1-10, doi:10.1149/1.2054684 (1994).
- 1159 82 Gruet, D., Delobel, B., Sicsic, D., Lucas, I. T. & Vivier, V. On the electrochemical impedance  
1160 response of composite insertion electrodes – Toward a better understanding of porous  
1161 electrodes. *Electrochim. Acta* **295**, 787-800, doi:10.1016/j.electacta.2018.10.115 (2019).
- 1162 83 Amatore, C. & Maisonhaute, E. When voltammetry reaches nanoseconds. *Anal. Chem.* **77**, 303A-  
1163 311A, doi:10.1021/ac053430m (2005).
- 1164 84 Popkirov, G. S. & Schindler, R. N. A New Impedance Spectrometer for the Investigation of  
1165 Electrochemical Systems. *Review of Scientific Instruments* **63**, 5366-5372, doi:Doi  
1166 10.1063/1.1143404 (1992).
- 1167 85 Wiegand, G., Neumaier, K. R. & Sackmann, E. Fast impedance spectroscopy: General aspects and  
1168 performance study for single ion channel measurements. *Rev Sci Instrum* **71**, 2309-2320,  
1169 doi:10.1063/1.1150447 (2000).

- 1170 86 Macdonald, J. R., Schoonman, J. & Lehen, A. P. Applicability and power of complex nonlinear  
1171 least squares for the analysis of impedance and admittance data. *J. Electroanal. Chem.* **131**, 77-  
1172 95, doi:10.1016/0022-0728(82)87062-9 (1982).
- 1173 87 *ZPlot For Windows*, <http://www.scribner.com/software/146-zplot-and-zview-for-windows>.  
1174 88 *ZSimpWin*, <https://www.ameteki.com/products/software/zsimpwin>.
- 1175 89 Box, G. E. P. & Draper, N. R. *Empirical Model-Building and Response Surfaces*. (Wiley, 1987).  
1176 90 Draper, N. R. & Smith, H., S. *Applied Regression Analysis*. (Wiley, 1981).  
1177 91 Orazem, M. E., Durbha, M., Deslouis, C., Takenouti, H. & Tribollet, B. Influence of surface  
1178 phenomena on the impedance response of a rotating disk electrode. *Electrochim. Acta* **44**, 4403-  
1179 4412, doi:Doi 10.1016/S0013-4686(99)00156-5 (1999).
- 1180 92 Brug, G. J., van den Eeden, A. L. G., Sluyters-Rehbach, M. & Sluyters, J. H. The Analysis of  
1181 Electrode Impedances Complicated by the Presence of a Constant Phase Element. *Journal of*  
1182 *Electroanalytical Chemistry* **176**, 275-295 (1984).
- 1183 93 Hirschorn, B. *et al.* Constant-Phase-Element Behavior Caused by Resistivity Distributions in  
1184 Films: I. Theory. *Journal of the Electrochemical Society* **157**, C452-C457 (2010).
- 1185 94 Wu, S. L., Orazem, M. E., Tribollet, B. & Vivier, V. The influence of coupled faradaic and charging  
1186 currents on impedance spectroscopy. *Electrochim Acta* **131**, 2-12 (2014).
- 1187 95 Gabrielli, C. & Group, S. I. *Identification of Electrochemical Processes by Frequency Response*  
1188 *Analysis*. (Solartron Electronic Group, 1980).
- 1189 96 Tuller, H. L., Litzelman, S. J. & Jung, W. Micro-ionics: next generation power sources. *Phys. Chem.*  
1190 *Chem. Phys.* **11**, 3023-3034 (2009).
- 1191 97 Huang, J. *et al.* Impedance Response of Porous Electrodes: Theoretical Framework, Physical  
1192 Models and Applications. *J. Electrochem. Soc.* **167**, doi:10.1149/1945-7111/abc655 (2020).  
1193 **A systematic review of physics-based EIS models for porous electrodes with substantial**  
1194 **mathematic details that may help model development.**
- 1195 98 Keddam, M., Mattos, O. R. & Takenouti, H. Reaction model for iron dissolution studied by  
1196 electrode impedance. II. Determination of the reaction model. *J. Electrochem. Soc.* **128**, 266-274,  
1197 doi:10.1149/1.2127402 (1981).
- 1198 99 Pivac, I. & Barbir, F. Inductive phenomena at low frequencies in impedance spectra of proton  
1199 exchange membrane fuel cells – A review. *J. Power Sources* **326**, 112-119,  
1200 doi:<https://doi.org/10.1016/j.jpowsour.2016.06.119> (2016).
- 1201 100 Roy, S. K., Orazem, M. E. & Tribollet, B. Interpretation of Low-Frequency Inductive Loops in PEM  
1202 Fuel Cells. *J. Electrochem. Soc.* **154**, doi:10.1149/1.2789377 (2007).
- 1203 101 Huang, J. *et al.* An Analytical Three-Scale Impedance Model for Porous Electrode with  
1204 Agglomerates in Lithium-Ion Batteries. *J. Electrochem. Soc.* **162**, A585-A595,  
1205 doi:10.1149/2.0241504jes (2015).
- 1206 102 Sabet, P. S. & Sauer, D. U. Separation of predominant processes in electrochemical impedance  
1207 spectra of lithium-ion batteries with nickel-manganese-cobalt cathodes. *J. Power Sources* **425**,  
1208 121-129 (2019).
- 1209 103 Boillot, M. *et al.* Effect of gas dilution on PEM fuel cell performance and impedance response.  
1210 *Fuel cells* **6**, 31-37 (2006).
- 1211 104 Harrington, D. A. & Conway, B. E. AC IMPEDANCE OF FARADAIC REACTIONS INVOLVING  
1212 ELECTROSORBED INTERMEDIATES .1. KINETIC-THEORY. *Electrochim. Acta* **32**, 1703-1712,  
1213 doi:10.1016/0013-4686(87)80005-1 (1987).  
1214 **A systematic methodology to construct EIS models from multi-step reaction mechanism.**
- 1215 105 Epelboin, I., Keddam, M. & Lestrade, J. C. Faradaic impedances and intermediates in  
1216 electrochemical reactions. *Faraday Discuss. Chem. Soc.* **56**, 264-275, doi:10.1039/dc9735600264  
1217 (1973).

- 1218 106 Gabrielli, C. & Keddam, M. Heterogeneous reactions coupled by diffusion. Multiple stationary  
1219 states, impedance, and stability. *J. Electroanal. Chem.* **45**, 267-277 (1973).
- 1220 107 Bertocci, U. & Ricker, R. E. in *ASTM Special Technical Publication*.1154 edn 143-161.
- 1221 108 Losiewicz, B., Jurczakowski, R. & Lasia, A. Kinetics of hydrogen underpotential deposition at  
1222 polycrystalline platinum in acidic solutions. *Electrochim. Acta* **80**, 292-301,  
1223 doi:10.1016/j.electacta.2012.07.019 (2012).
- 1224 109 Wang, S. S., Sun, Y., Huang, F. S. & Zhang, J. B. Freezing Site of Super-Cooled Water and Failure  
1225 Mechanism of Cold Start of PEFC. *Journal of the Electrochemical Society* **166**, F860-F864,  
1226 doi:10.1149/2.0041913jes (2019).
- 1227 110 Takahashi, M., Tobishima, S., Takei, K. & Sakurai, Y. Reaction behavior of LiFePO<sub>4</sub> as a cathode  
1228 material for rechargeable lithium batteries. *Solid State Ion.* **148**, 283-289, doi:10.1016/s0167-  
1229 2738(02)00064-4 (2002).
- 1230 111 Vieil, E., Maurey-Mey, M. & Cauquis, G. Current log-transform vs reactant concentration as a  
1231 tool for chemical reaction order and electrochemical mechanisms determination—I. General  
1232 theory in steady-state voltammetry and application to electro-oxidation of thianthrene in  
1233 presence of water. *Electrochim. Acta* **27**, 1565-1583, doi:10.1016/0013-4686(82)80083-2 (1982).
- 1234 112 Laidler, K. J. The development of the Arrhenius equation. *Journal of Chemical Education* **61**, 494,  
1235 doi:10.1021/ed061p494 (1984).
- 1236 113 Hong, P., Xu, L. F., Jiang, H. L., Li, J. Q. & Ouyang, M. G. A new approach to online AC impedance  
1237 measurement at high frequency of PEM fuel cell stack. *Int. J. Hydrog. Energy* **42**, 19156-19169,  
1238 doi:10.1016/j.ijhydene.2017.06.035 (2017).
- 1239 114 Zhu, J. G., Sun, Z. C., Wei, X. Z. & Dai, H. F. A new lithium-ion battery internal temperature on-  
1240 line estimate method based on electrochemical impedance spectroscopy measurement. *J.*  
1241 *Power Sources* **274**, 990-1004, doi:10.1016/j.jpowsour.2014.10.182 (2015).
- 1242 115 Khan, M. Z. H., Hasan, M. R., Hossain, S. I., Ahommed, M. S. & Daizy, M. Ultrasensitive detection  
1243 of pathogenic viruses with electrochemical biosensor: State of the art. *Biosens Bioelectron* **166**,  
1244 112431, doi:10.1016/j.bios.2020.112431 (2020).
- 1245 116 Prodromidis, M. I. Impedimetric immunosensors-A review. *Electrochim. Acta* **55**, 4227-4233,  
1246 doi:10.1016/j.electacta.2009.01.081 (2010).
- 1247 117 Seven, B. *et al.* Impedimetric biosensor for cancer cell detection. *Electrochem. Commun.* **37**, 36-  
1248 39, doi:10.1016/j.elecom.2013.10.003 (2013).
- 1249 118 Abe, T., Sagane, F., Ohtsuka, M., Iriyama, Y. & Ogumi, Z. Lithium-ion transfer at the interface  
1250 between lithium-ion conductive ceramic electrolyte and liquid electrolyte - A key to enhancing  
1251 the rate capability of lithium-ion batteries. *J. Electrochem. Soc.* **152**, A2151-A2154,  
1252 doi:10.1149/1.2042907 (2005).
- 1253 119 Song, H.-K., Jung, Y.-H., Lee, K.-H. & Dao, L. H. Electrochemical impedance spectroscopy of  
1254 porous electrodes: the effect of pore size distribution. *Electrochim. Acta* **44**, 3513-3519 (1999).
- 1255 120 Song, H.-K., Hwang, H.-Y., Lee, K.-H. & Dao, L. H. The effect of pore size distribution on the  
1256 frequency dispersion of porous electrodes. *Electrochim. Acta* **45**, 2241-2257 (2000).
- 1257 121 Suthar, B., Landesfeind, J., Eldiven, A. & Gasteiger, H. A. Method to Determine the In-Plane  
1258 Tortuosity of Porous Electrodes. *Journal of the Electrochemical Society* **165**, A2008-A2018,  
1259 doi:10.1149/2.0121810jes (2018).
- 1260 122 Ritter, S. *et al.* Results of an international round-robin exercise on electrochemical impedance  
1261 spectroscopy. *Corrosion Engineering, Science and Technology*, 1-15,  
1262 doi:10.1080/1478422X.2020.1850070 (2020).
- 1263 123 Tait, W. S. Using Electrochemical Measurements to Estimate Coating and Polymer Film  
1264 Durability. *Journal of Coatings Technology* **75**, 45-50 (2003).

- 1265 124 Tait, W. S. Using electrochemical measurements to estimate coating and polymer film durability. *Journal of Coatings Technology* **75**, 45-50, doi:Doi 10.1007/Bf02730070 (2003).  
1266
- 1267 125 Boukamp, B. A. A Linear Kronig - Kramers Transform Test for Immittance Data Validation. *J. Electrochem. Soc.* **142**, 1885-1894, doi:10.1149/1.2044210 (1995).  
1268
- 1269 126 You, C., Zabara, M. A., Orazem, M. E. & Ulgut, B. Application of the Kramers–Kronig Relations to  
1270 Multi-Sine Electrochemical Impedance Measurements. *Journal of The Electrochemical Society*  
1271 **167**, 020515, doi:10.1149/1945-7111/ab6824 (2020).
- 1272 127 Allagui, A., Freeborn, T. J., Elwakil, A. S. & Maundy, B. J. Reevaluation of Performance of Electric  
1273 Double-layer Capacitors from Constant-current Charge/Discharge and Cyclic Voltammetry. *Sci*  
1274 *Rep* **6**, 38568, doi:10.1038/srep38568 (2016).  
1275 **A detailed description of the use of a constant-phase element in cyclic voltammetry.**
- 1276 128 Gharbi, O., Tran, M. T. T., Tribollet, B., Turmine, M. & Vivier, V. Revisiting cyclic voltammetry and  
1277 electrochemical impedance spectroscopy analysis for capacitance measurements. *Electrochim.*  
1278 *Acta* **343**, 136109, doi:10.1016/j.electacta.2020.136109 (2020).
- 1279 129 Sadkowski, A. Time domain responses of constant phase electrodes. *Electrochim Acta* **38**, 2051-  
1280 2054, doi:[http://dx.doi.org/10.1016/0013-4686\(93\)80339-2](http://dx.doi.org/10.1016/0013-4686(93)80339-2) (1993).
- 1281 130 Sadkowski, A. On the ideal polarisability of electrodes displaying cpe-type capacitance  
1282 dispersion. *J. Electroanal. Chem.* **481**, 222-226, doi:10.1016/s0022-0728(99)00480-5 (2000).  
1283 **This article discusses the physical meaning of constant phase element.**
- 1284 131 Newman, J. Frequency dispersion in capacity measurements at a disk electrode. *Journal of the*  
1285 *Electrochemical Society* **117**, 198-203 (1970).
- 1286 132 Huang, V. M.-W., Vivier, V., Frateur, I., Orazem, M. E. & Tribollet, B. The global and local  
1287 impedance response of a blocking disk electrode with local constant-phase-element behavior. *J.*  
1288 *Electrochem. Soc.* **154**, C89-C98 (2007).
- 1289 133 Huang, V. M.-W., Vivier, V., Orazem, M. E., Pebere, N. & Tribollet, B. The apparent constant-  
1290 phase-element behavior of a disk electrode with Faradaic reactions. A global and local  
1291 impedance analysis. *J. Electrochem. Soc.* **154**, C99-C107 (2007).
- 1292 134 Orazem, M. E. *et al.* Dielectric Properties of Materials Showing Constant-Phase-Element (CPE)  
1293 Impedance Response. *J. Electrochem. Soc.* **160**, C215-C225, doi:10.1149/2.033306jes (2013).  
1294 **Overview of methods used to extract capacitance from CPE parameters, with emphasis on the**  
1295 **use of a power-law model to extract thickness of oxide films.**
- 1296 135 Hirschorn, B. *et al.* Determination of effective capacitance and film thickness from constant-  
1297 phase-element parameters. *Electrochim Acta* **55**, 6218-6227 (2010).
- 1298 136 Hirschorn, B. *et al.* Constant-Phase-Element Behavior Caused by Resistivity Distributions in  
1299 Films: II. Applications. *Journal of the Electrochemical Society* **157**, C458-C463 (2010).
- 1300 137 Díaz, B., Guitián, B., Nóvoa, X. R. & Pérez, M. C. The effect of chlorides on the corrosion  
1301 behaviour of weathered reinforcing bars. *Electrochim. Acta* **336**, 135737,  
1302 doi:10.1016/j.electacta.2020.135737 (2020).
- 1303 138 Hernández, R. D. P. B., Aoki, I. V., Tribollet, B. & De Melo, H. G. Electrochemical impedance  
1304 spectroscopy investigation of the electrochemical behaviour of copper coated with artificial  
1305 patina layers and submitted to wet and dry cycles. *Electrochim Acta* **56**, 2801-2814,  
1306 doi:10.1016/j.electacta.2010.12.059 (2011).
- 1307 139 Capelossi, V. R. *et al.* Corrosion protection of clad 2024 aluminum alloy anodized in tartaric-  
1308 sulfuric acid bath and protected with hybrid sol-gel coating. *Electrochim. Acta* **124**, 69-79,  
1309 doi:10.1016/j.electacta.2013.09.004 (2014).
- 1310 140 Bouali, A. C. *et al.* Layered double hydroxide based active corrosion protective sealing of plasma  
1311 electrolytic oxidation/sol-gel composite coating on AA2024. *Applied Surface Science* **494**, 829-  
1312 840, doi:10.1016/j.apsusc.2019.07.117 (2019).

- 1313 141 Calado, L. M., Taryba, M. G., Carmezim, M. J. & Montemor, M. F. Self-healing ceria-modified  
1314 coating for corrosion protection of AZ31 magnesium alloy. *Corros Sci* **142**, 12-21,  
1315 doi:10.1016/j.corsci.2018.06.013 (2018).
- 1316 142 Roggero, A. *et al.* Thermal activation of impedance measurements on an epoxy coating for the  
1317 corrosion protection: 2. electrochemical impedance spectroscopy study. *Electrochim. Acta* **305**,  
1318 116-124, doi:10.1016/j.electacta.2019.03.007 (2019).
- 1319 143 Karden, E., Buller, S. & De Doncker, R. W. A method for measurement and interpretation of  
1320 impedance spectra for industrial batteries. *J. Power Sources* **85**, 72-78, doi:Doi 10.1016/S0378-  
1321 7753(99)00385-7 (2000).
- 1322 144 Costard, J., Ender, M., Weiss, M. & Ivers-Tiffée, E. Three-Electrode Setups for Lithium-Ion  
1323 Batteries: II. Experimental Study of Different Reference Electrode Designs and Their Implications  
1324 for Half-Cell Impedance Spectra. *Journal of The Electrochemical Society* **164**, A80-A87,  
1325 doi:10.1149/2.0241702jes (2017).
- 1326 145 Osaka, T., Mukoyama, D. & Nara, H. Review—Development of Diagnostic Process for  
1327 Commercially Available Batteries, Especially Lithium Ion Battery, by Electrochemical Impedance  
1328 Spectroscopy. *J. Electrochem. Soc.* **162**, A2529-A2537, doi:10.1149/2.0141514jes (2015).
- 1329 146 Itou, Y., Ogihara, N. & Kawauchi, S. Role of Conductive Carbon in Porous Li-Ion Battery  
1330 Electrodes Revealed by Electrochemical Impedance Spectroscopy Using a Symmetric Cell. *J Phys*  
1331 *Chem C* **124**, 5559-5564, doi:10.1021/acs.jpcc.9b11929 (2020).
- 1332 147 Ji, G., Macia, L. F., Allaert, B., Hubin, A. & Terryn, H. Odd Random Phase Electrochemical  
1333 Impedance Spectroscopy to Study the Corrosion Behavior of Hot Dip Zn and Zn-Alloy Coated  
1334 Steel Wires in Sodium Chloride Solution. *Journal of the Electrochemical Society* **165**, C246-C257,  
1335 doi:10.1149/2.0741805jes (2018).
- 1336 148 Sanchez, B., Fernandez, X., Reig, S. & Bragos, R. An FPGA-based frequency response analyzer for  
1337 multisine and stepped sine measurements on stationary and time-varying impedance.  
1338 *Measurement Science and Technology* **25**, doi:10.1088/0957-0233/25/1/015501 (2014).
- 1339 149 Gabrielli, C., Huet, F. & Keddam, M. Comparison of sine wave and white noise analysis for  
1340 electrochemical impedance measurements. *J. Electroanal. Chem.* **335**, 33-53, doi:10.1016/0022-  
1341 0728(92)80230-2 (1992).
- 1342 150 Chang, B. Y. & Park, S. M. in *Annual Review of Analytical Chemistry* Vol. 3 207-229 (2010).
- 1343 151 Smulko, J. M., Darowicki, K. & Zielinski, A. On Electrochemical Noise Analysis for Monitoring of  
1344 Uniform Corrosion Rate. *IEEE Transactions on Instrumentation and Measurement* **56**, 2018-  
1345 2023, doi:10.1109/TIM.2007.895624 (2007).
- 1346 152 Cottis, R. A. Interpretation of electrochemical noise data. *Corrosion* **57**, 265-285, doi:Doi  
1347 10.5006/1.3290350 (2001).
- 1348 153 Abada, S. *et al.* Safety focused modeling of lithium-ion batteries: A review. *J. Power Sources* **306**,  
1349 178-192, doi:10.1016/j.jpowsour.2015.11.100 (2016).
- 1350 154 Deslouis, C., Tribollet, B., Mengoli, G. & Musiani, M. M. Electrochemical behavior of copper in  
1351 neutral aerated chloride solution. II. Impedance investigation. *Journal of Applied*  
1352 *Electrochemistry* **18**, 384-393, doi:10.1007/bf01093752 (1988).
- 1353 **A comprehensive analysis of EIS and transfer functions applied to the corrosion of copper in**  
1354 **chloride solution.**
- 1355 155 Robertson, B., Tribollet, B. & Deslouis, C. Measurement of Diffusion Coefficients by DC and EHD  
1356 Electrochemical Methods. *J. Electrochem. Soc.* **135**, 2279-2284, doi:10.1149/1.2096252 (1988).
- 1357 156 Tribollet, B., Newman, J. & Smyrl, W. H. Determination of the Diffusion Coefficient from  
1358 Impedance Data in the Low Frequency Range. *J. Electrochem. Soc.* **135**, 134-138,  
1359 doi:10.1149/1.2095539 (1988).

- 1360 157 Antano-Lopez, R., Keddami, M. & Takenouti, H. A new experimental approach to the time-  
1361 constants of electrochemical impedance: frequency response of the double layer capacitance.  
1362 *Electrochim. Acta* **46**, 3611-3617, doi:Doi 10.1016/S0013-4686(01)00640-5 (2001).
- 1363 158 Cachet, H. *et al.* Capacitance probe of the electron displacement in a dye sensitized solar cell by  
1364 an intermodulation technique: a quantitative model. *Electrochim. Acta* **49**, 2541-2549 (2004).
- 1365 159 Larios-Duran, E. R. *et al.* Dynamics of double-layer by AC Modulation of the Interfacial  
1366 Capacitance and Associated Transfer Functions. *Electrochim. Acta* **55**, 6292-6298,  
1367 doi:10.1016/j.electacta.2009.10.036 (2010).
- 1368 160 Antaño-López, R., Keddami, M., Turmine, M. & Vivier, V. The Impedance Response of a Passive  
1369 Film Revisited by a Double Modulation Technique. *ChemElectroChem* **6**, 202-210,  
1370 doi:10.1002/celec.201800737 (2019).
- 1371 161 Zou, F., Thierry, D. & Isaacs, H. S. A high-resolution probe for localized electrochemical  
1372 impedance spectroscopy measurements. *J. Electrochem. Soc.* **144**, 1957-1965, doi:Doi  
1373 10.1149/1.1837729 (1997).
- 1374 **This study reports the design of dual microelectrodes for performing local EIS for enhancing**  
1375 **the spatial resolution of the technique.**
- 1376 162 Ferrari, J. V. *et al.* Influence of normal and radial contributions of local current density on local  
1377 electrochemical impedance spectroscopy. *Electrochim. Acta* **60**, 244-252,  
1378 doi:10.1016/j.electacta.2011.11.053 (2012).
- 1379 163 de Abreu, C. P. *et al.* Multiscale Electrochemical Study of Welded Al Alloys Joined by Friction Stir  
1380 Welding. *J. Electrochem. Soc.* **164**, C735-C746, doi:10.1149/2.0391713jes (2017).
- 1381 164 Shkirskiy, V., Volovitch, P. & Vivier, V. Development of quantitative Local Electrochemical  
1382 Impedance Mapping: an efficient tool for the evaluation of delamination kinetics. *Electrochim.*  
1383 *Acta* **235**, 442-452, doi:10.1016/j.electacta.2017.03.076 (2017).
- 1384 165 Gharbi, O., Ngo, K., Turmine, M. & Vivier, V. Local electrochemical impedance spectroscopy: A  
1385 window into heterogeneous interfaces. *Current Opinion in Electrochemistry* **20**, 1-7,  
1386 doi:10.1016/j.coelec.2020.01.012 (2020).
- 1387 166 Creason, S. C. & Smith, D. E. Fourier transform Faradaic admittance measurements: I.  
1388 Demonstration of the applicability of random and pseudo-random noise as applied potential  
1389 signals. *J. Electroanal. Chem.* **36**, A1-A7 (1972).
- 1390 167 Dokko, K. *et al.* Kinetic characterization of single particles of LiCoO<sub>2</sub> by AC impedance and  
1391 potential step methods. *J. Electrochem. Soc.* **148**, A422-A426, doi:10.1149/1.1359197 (2001).
- 1392 168 Stoyanov, Z. B. & Savova-Stoyanov, B. S. Impedance study of non-stationary systems: four-  
1393 dimensional analysis. *J. Electroanal. Chem.* **183**, 133-144, doi:[https://doi.org/10.1016/0368-  
1394 1874\(85\)85486-1](https://doi.org/10.1016/0368-1874(85)85486-1) (1985).
- 1395 169 Itagaki, M. *et al.* In situ electrochemical impedance spectroscopy to investigate negative  
1396 electrode of lithium-ion rechargeable batteries. *J. Power Sources* **135**, 255-261,  
1397 doi:10.1016/j.jpowsour.2004.04.004 (2004).
- 1398 170 Huang, J., Li, Z. & Zhang, J. B. Dynamic electrochemical impedance spectroscopy reconstructed  
1399 from continuous impedance measurement of single frequency during charging/discharging. *J.*  
1400 *Power Sources* **273**, 1098-1102, doi:10.1016/j.jpowsour.2014.07.067 (2015).
- 1401 171 Wiezell, K., Holmstrom, N. & Lindbergh, G. Studying Low-Humidity Effects in PEFCs Using EIS II.  
1402 Modeling. *J. Electrochem. Soc.* **159**, F379-F392, doi:10.1149/2.006208jes (2012).
- 1403 172 Setzler, B. P. & Fuller, T. F. A Physics-Based Impedance Model of Proton Exchange Membrane  
1404 Fuel Cells Exhibiting Low-Frequency Inductive Loops. *J. Electrochem. Soc.* **162**, F519-F530,  
1405 doi:10.1149/2.0361506jes (2015).

- 1406 173 Kulikovskiy, A. A. Analysis of Damjanovic kinetics of the oxygen reduction reaction: Stability,  
1407 polarization curve and impedance spectra. *J. Electroanal. Chem.* **738**, 130-137,  
1408 doi:10.1016/j.jelechem.2014.11.014 (2015).
- 1409 174 Schneider, I. A., Kramer, D., Wokaun, A. & Scherer, G. G. Oscillations in gas channels - II.  
1410 Unraveling the characteristics of the low frequency loop in air-fed PEFC impedance spectra. *J.*  
1411 *Electrochem. Soc.* **154**, B770-B782, doi:10.1149/1.2742291 (2007).
- 1412 175 Kuhn, H., Andreaus, B., Wokaun, A. & Scherer, G. G. Electrochemical impedance spectroscopy  
1413 applied to polymer electrolyte fuel cells with a pseudo reference electrode arrangement.  
1414 *Electrochim. Acta* **51**, 1622-1628, doi:10.1016/j.electacta.2005.02.108 (2006).
- 1415 176 Raccichini, R., Amores, M. & Hinds, G. Critical Review of the Use of Reference Electrodes in Li-Ion  
1416 Batteries: A Diagnostic Perspective. *Batteries-Basel* **5**, 24, doi:10.3390/batteries5010012 (2019).
- 1417 177 Hoshi, Y. *et al.* Optimization of reference electrode position in a three-electrode cell for  
1418 impedance measurements in lithium-ion rechargeable battery by finite element method. *J.*  
1419 *Power Sources* **288**, 168-175, doi:10.1016/j.jpowsour.2015.04.065 (2015).
- 1420 178 Solchenbach, S., Pritzl, D., Kong, E. J. Y., Landesfeind, J. & Gasteiger, H. A. A gold micro-reference  
1421 electrode for impedance and potential measurements in lithium ion batteries. *Journal of The*  
1422 *Electrochemical Society* **163**, A2265 (2016).
- 1423 179 Chu, Z. Y. *et al.* Testing Lithium-Ion Battery with the Internal Reference Electrode: An Insight into  
1424 the Blocking Effect. *Journal of the Electrochemical Society* **165**, A3240-A3248,  
1425 doi:10.1149/2.0141814jes (2018).
- 1426 180 Orazem, M. E. Electrochemical impedance spectroscopy: the journey to physical understanding.  
1427 *Journal of Solid State Electrochemistry* **24**, 2151-2153, doi:10.1007/s10008-020-04725-9 (2020).
- 1428 181 Agarwal, P., Orazem, M. E. & Garci-Rubio, L. H. Measurement models for electrochemical  
1429 impedance spectroscopy. I. Demonstration of applicability. *J. Electrochem. Soc.* **139**, 1917-1927  
1430 (1992).
- 1431 182 Liao, H. *et al.* Physical Properties Obtained from Measurement Model Analysis of Impedance  
1432 Measurements. *Electrochimica Acta* **354**, 136747 (2020).

1433

1434

1435 REVIEWER ACCREDITATION INFORMATION

1436 *Nature Reviews Methods Primers* thanks I. Shitanda, A. Lasia and S. Ciampi for their contribution to the  
1437 peer review of this work.

1438

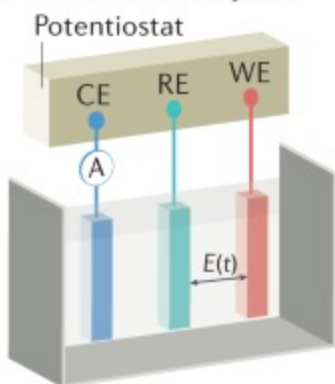
1439 TABLE OF CONTENTS BLURB

1440 This Primer on electrochemical impedance spectroscopy (EIS) provides a guide to experimental design to  
1441 measure impedance and how these data are analyzed. The range of applications that require EIS from  
1442 measuring battery performance to electrochemical biosensors are highlighted. Limitations of the  
1443 method along with emerging trends in experimental optimizations and data interpretation are also  
1444 described.

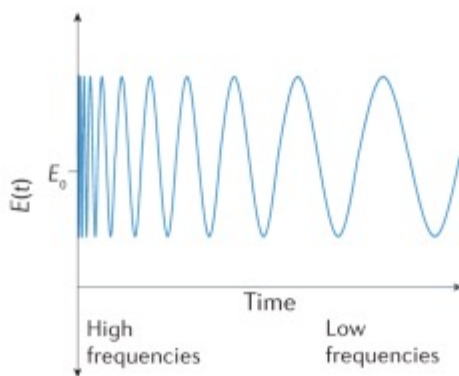
1445

Fig. 1

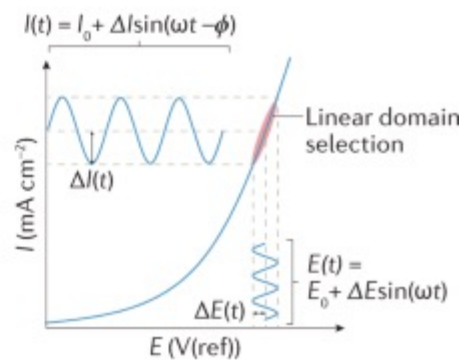
**a Electrochemical system**



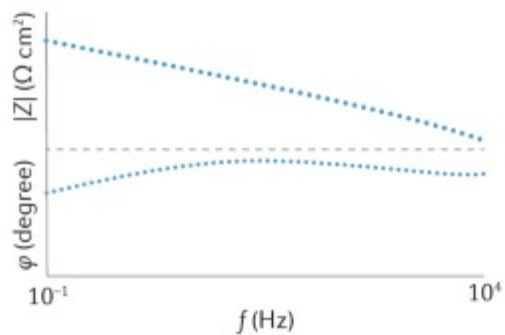
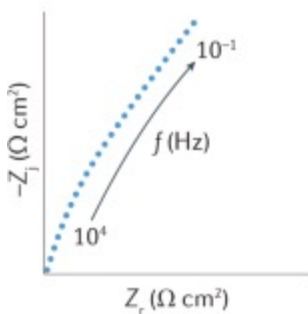
**b Perturbation signal**



**c Electrochemical response**



**d Graphical representation**



**e Equivalent circuit and model**

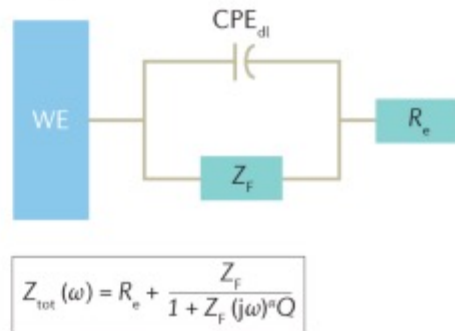


Fig. 2

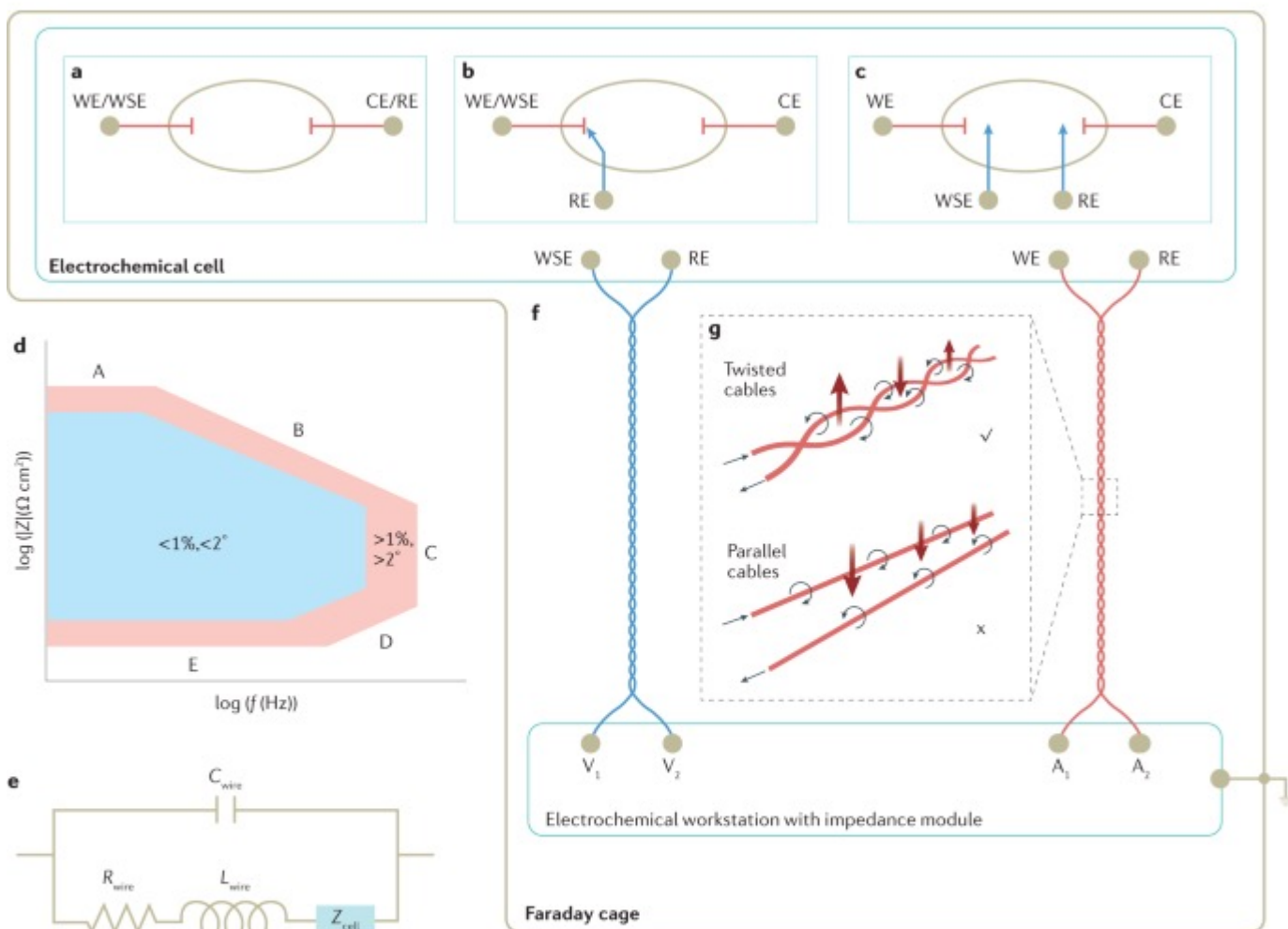


Fig. 3

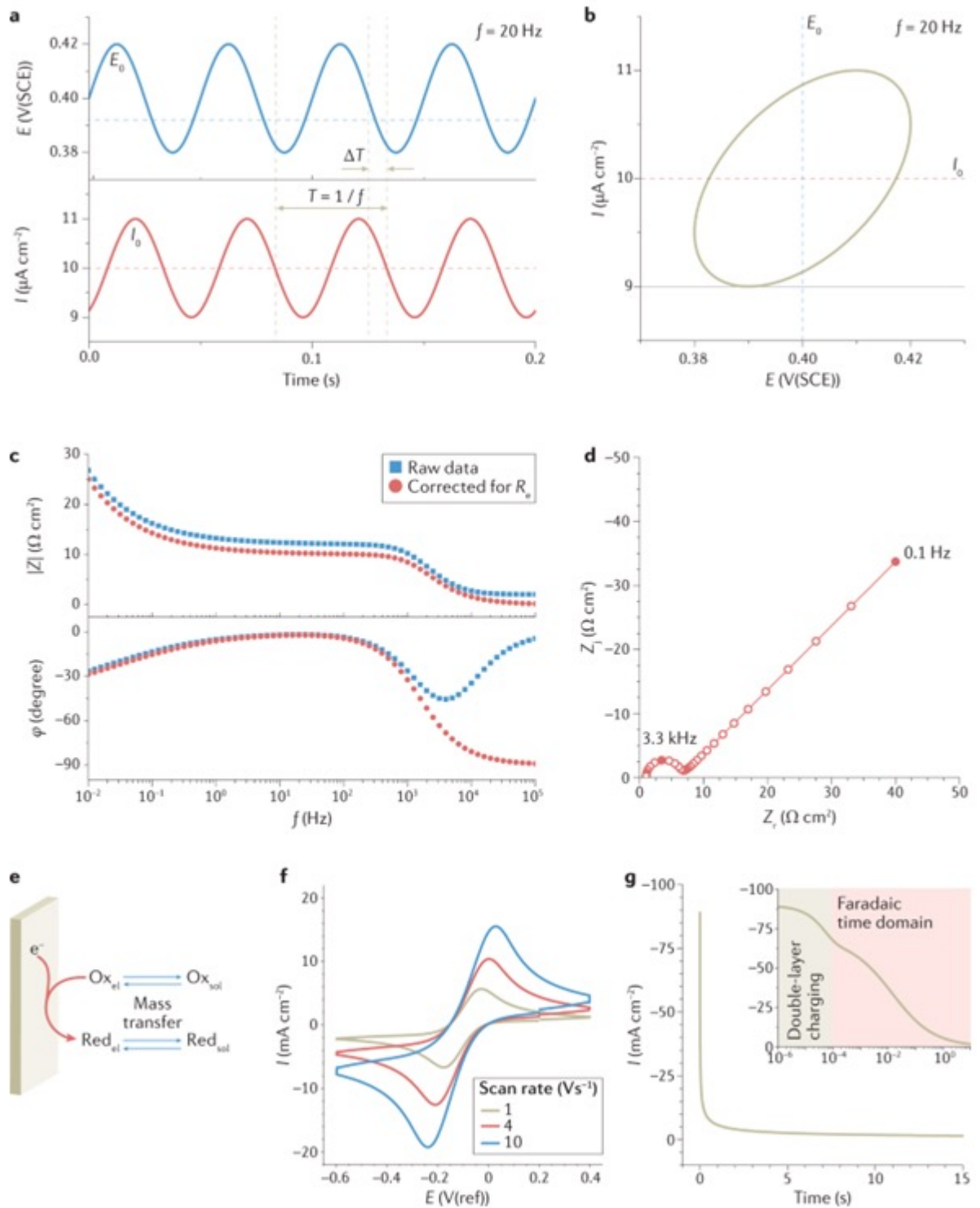


Fig. 4

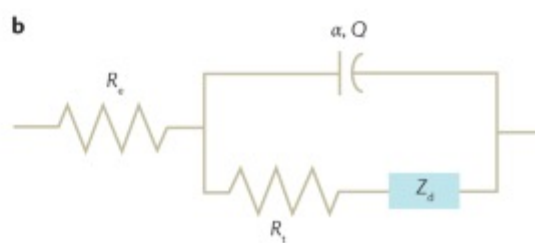
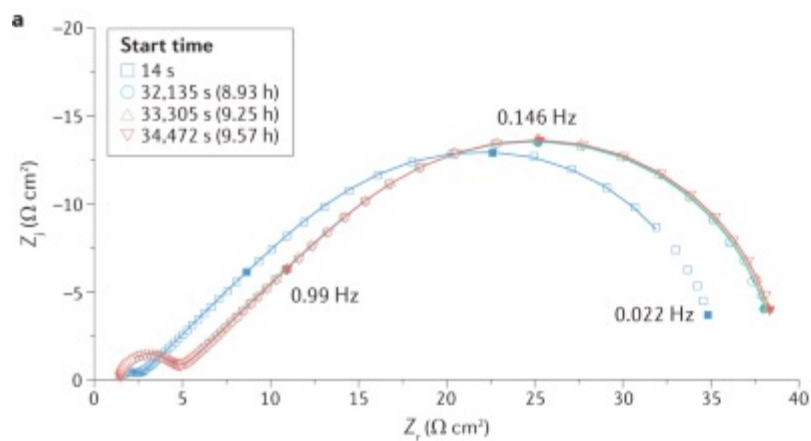
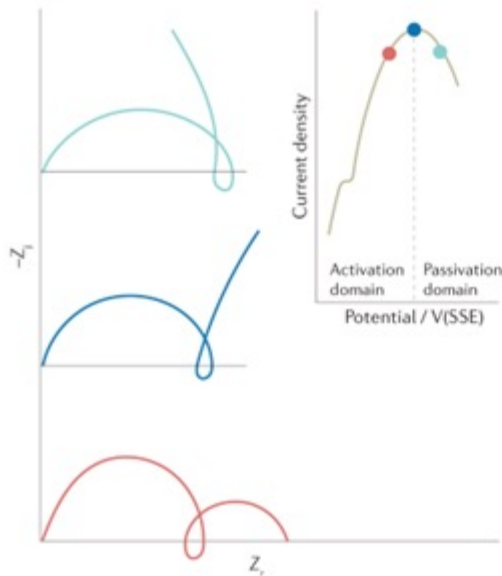
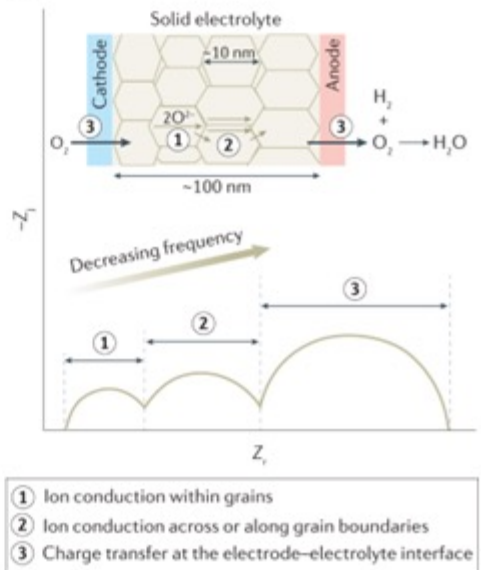


Fig. 5.

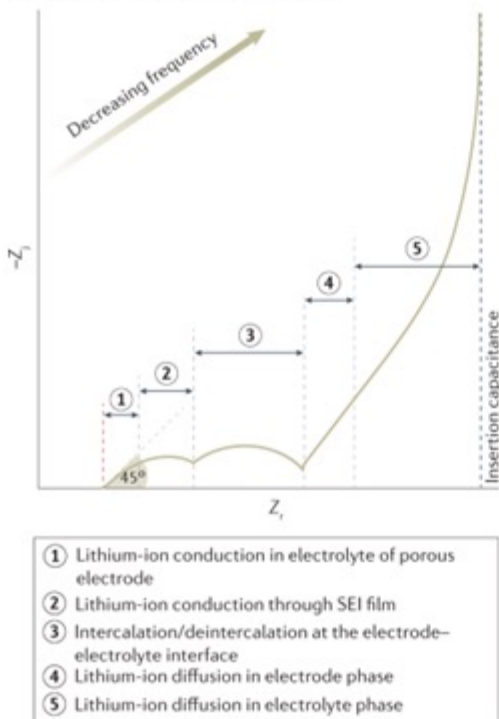
**a Typical EIS of iron corrosion in sulfuric acid solution**



**b Typical EIS of solid oxide fuel cells**



**c Typical EIS of lithium-ion batteries**



**d Typical EIS of polymer electrolyte fuel cells**

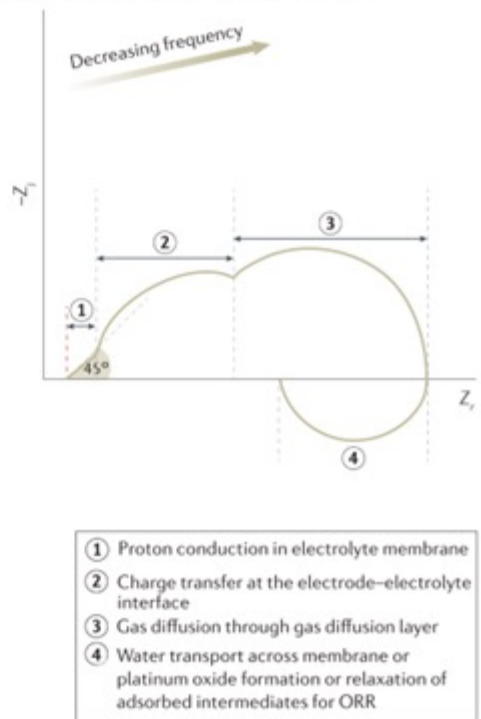


Fig. 6

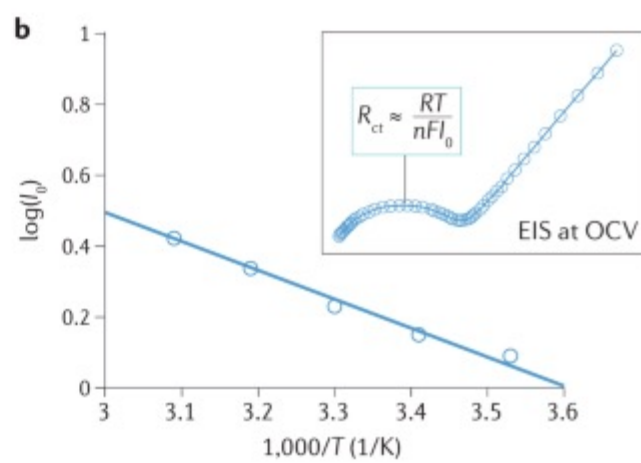
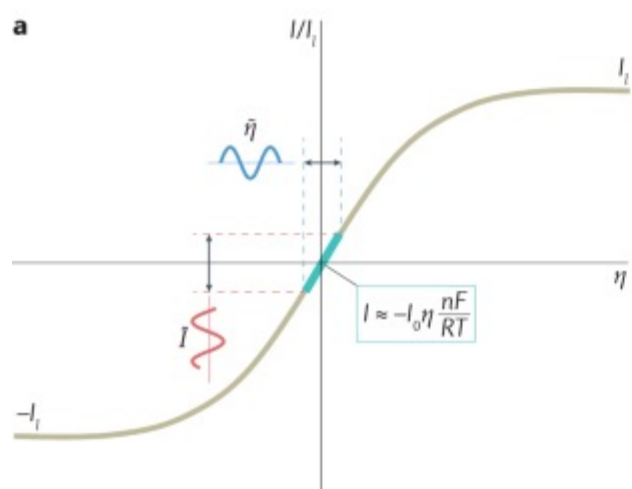


Fig. 7

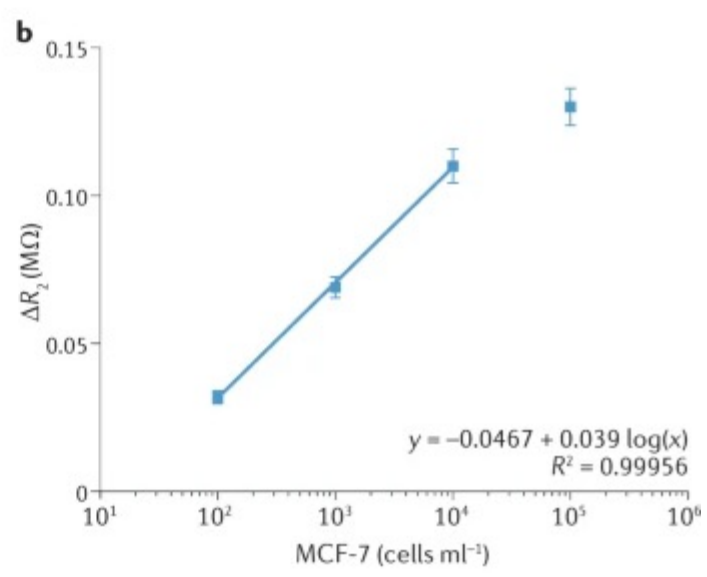
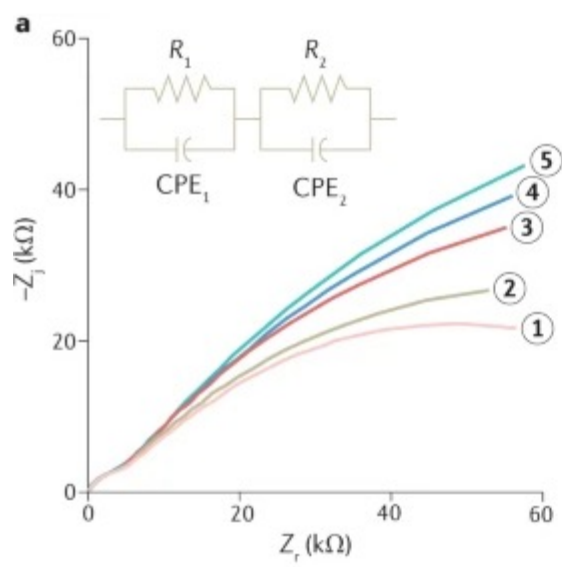


Fig. 8

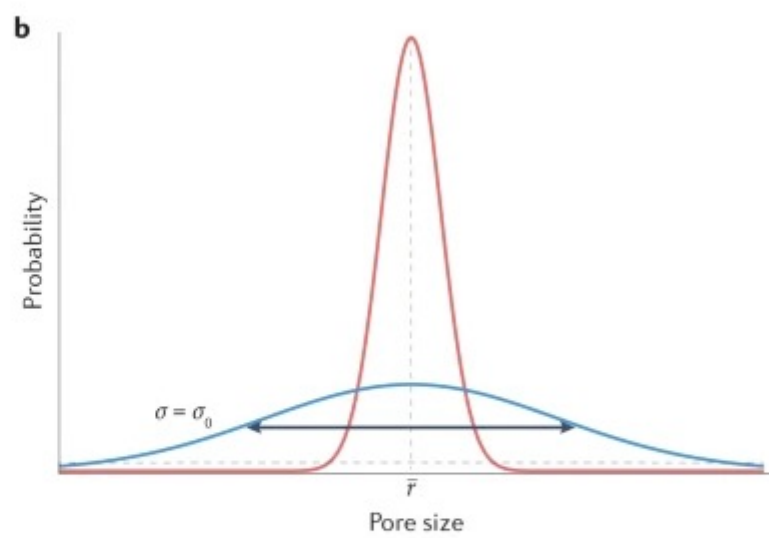
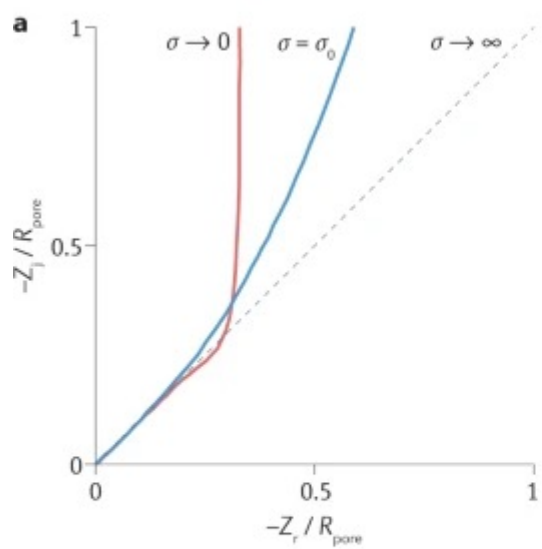


Fig. 9

